in-situ Observations of Ionospheric Plasma Blobs Over Nigeria (9.08ºN, 8.67ºE) During Deep Solar Minimum: Possible Influence of Small-Scale Fluctuations in Ionospheric Plasma Density

Oluwasegun M. Adebayo[1*], Babatunde Rabiu[2], Kazuo Shiokawa[3], Daniel I. Okoh[2], Aderonke A. Obafaye[2], Alexandre A. Pimenta[1], Yuichi Otsuka[3] and Oluwakemi E. Dare-Idowu[2]

[1]Heliophysics, Planetary Science and Aeronomy Division, National Institute for Space Research (INPE), São José dos Campos 12227-010, Brazil.

[2]United Nations African Regional Centre for Space Science Technology and Education - English, (UN-ARCSSTE-E), Obafemi Awolowo University Campus, Ile Ife, Nigeria.

[3] Institute for Space-Earth Environmental Research, Nagoya University, Nagoya, Japan.

Corresponding author: Oluwasegun Adebayo (oluwasegun.adebayo@inpe.br)

Key Points:

- 58% of the blobs were observed in the absence of bubbles in the vicinity of Africa and South America.
- Blobs associated with small-scale fluctuations are more disturbed than the ones without.
- The rate of change of the electron density inside the blobs associated with small-scale fluctuations is ~50% above that of the blobs without.

Abstract

Ionospheric plasma blobs have long been studied since it was first reported in 1986. Blobs are localized regions of enhanced plasma with a factor of 2 or 3 above ambient plasma. In this paper, we studied the occurrence of blobs over Nigeria (9.08ºN, 8.67ºE geographic coordinates) using the SWARM constellation satellites – ionospheric plasma density dataset specifically. We considered only the nighttime pass of the satellites over Nigeria with time frame 18:00 to 04:59 LT. The satellites passed over Nigeria 126 times in 2019 with 41 cases of plasma blobs. The results show that 58% of the cases were found without bubbles nearby, 29% of the cases were found in the presence of small-scale fluctuations in ionospheric plasma density (henceforth "SSFiI"). From the spectral analysis, the average wavelength, period and the propagating speed of SSFiI are 11 km, 2-4 seconds, and 2.75 – 5.5 km/s, respectively. The rate of change of the electron density inside the blobs associated with SSFiI was ~50% above that of the blobs in the absence of SSFiI. This suggests that bubbles may not be the only prerequisite for the development and dynamics of blobs; and SSFiI may play a significant role in the morphology and dynamics of blobs.

Plain Language Summary

This study investigates ionospheric plasma blobs over Nigeria using SWARM constellation satellites. We focused on nighttime passes in 2019 and identified 41 cases of plasma blobs out of 126 satellite passes. Surprisingly, 58% occurred without nearby bubbles, challenging the belief that bubbles are essential for blob formation. Additionally, 29% of cases showed small-scale fluctuations in ionospheric plasma density (SSFiI). Spectral analysis revealed SSFiI's predominant signal in the 2-4 seconds period and propagating speed of 2.75 – 5.5 km/s. Notably, blobs with SSFiI had a ~50% higher electron density change than those without. This suggests SSFiI may significantly influence blob morphology and dynamics, questioning the exclusive role of bubbles in blob development.

Keywords: plasma blobs, plasma bubbles, solar minimum, SSFiI, SWARM

1.0 Introduction

Plasma blobs, observed in various forms of plasma such as ionospheric plasma (Park et al., 2022), solar plasma (Patel et al., 2020), magnetospheric plasma (De Keyser et al., 2001), and laboratory plasma (Majeski et al., 2021), are ubiquitous in plasma studies. These plasma "balls" with

significant mass and energy above their surroundings have been extensively studied, with a specific focus on ionospheric plasma blobs in this paper (Kil et al., 2019; Park et al., 2022; Watanabe & Oya, 1986). Ionospheric blobs are localized regions of enhanced plasma, typically exhibiting 2 or 3 factors above ambient plasma levels.

The relationship between ionospheric plasma blobs and other phenomena such as plasma bubbles, MSTID, geomagnetic storms, and EIA has been established through observational studies (Adebayo et al., 2023; Agyei-Yeboah et al., 2021; Tardelli-Coelho et al., 2017; Kil et al., 2019; Pimenta et al., 2007; Park et al., 2022). Notably, the co-occurrence and distribution similarities of bubbles and blobs at the same magnetic meridian (Huang et al., 2014; Yokoyama et al., 2007) and numerical simulations supporting blob formation during bubble development (Krall et al., 2010) suggest a close relationship. However, the detection of blobs in the absence of bubbles indicates that bubbles are not a necessary precondition for blob formation (Klenzing et al., 2011). Similar observational studies linking MSTIDs and blobs, as well as their climatological occurrence patterns, further support the idea that these blobs are associated with these phenomena (Kil et al., 2019; Miller et al., 2014; Haaser et al., 2012).

Researchers have explored mechanisms underlying plasma blob formation. One hypothesis suggests a link between blob formation and the dynamics of bubble structures, wherein the enhancement of the polarization E-field within bubbles serves as a metaphorical "ball" undergoing poleward reflections, ultimately leading to the formation of plasma blobs (Huang et al., 2014; Krall et al., 2010; Park et al., 2003). An alternative hypothesis proposes that meridional winds and nonuniform airflow patterns in the ionosphere can alter the spatial distribution of plasma density within a bubble flux tube, resulting in the manifestation of plasma density enhancements or "blobs" (Wang et al., 2019; Klenzing et al., 2011).

It's noteworthy that some regions, such as Africa, exhibit plasma bubbles without associated plasma blobs (Okoh et al., 2017; Adebayo, 2021). However, recent case studies over Africa by Park et al. (2022b) associated plasma blob occurrences with the activities of the EIA, showcasing in situ plasma density enhancements correlated with patch-like increases in GOLD nightglow intensity using LEO satellites. These blobs were found to stay close to the EIA crest region and

poleward of nearby bubbles, consistent with earlier studies in Central/South America (Park et al., 2022).

In this paper, we present the first in-situ observations of ionospheric plasma blobs over Nigeria during a deep solar minimum. While extensive literature exists over the Brazilian tropical sector, studies over Africa, especially Nigeria, are limited. This research aims to scrutinize the morphology and dynamics of these blobs and assess the possible influence of small-scale fluctuations in ionospheric plasma density. Using ESA SWARM constellation satellites, we conducted a comprehensive study, considering only nighttime passes over Nigeria in 2019. Our results include occurrence patterns, classifications of blob signatures, spectral and statistical analyses.

2.0 Instruments

2.1 SWARM constellation

Swarm is a constellation mission by the European Space Agency (ESA) consisting of three identical satellites, namely Swarm A, B, and C, launched into near-polar orbits in November 2013. Their initial pearl-of-strings configuration allowed for the study of PCP evolution, as Spicher et al. (2015) explained. By April 2014, the satellites' orbits had drifted, resulting in Swarm A and Swarm C orbiting at about 460 km and Swarm B at approximately 510 km. Each swarm satellite carries an identical payload comprising several instruments; in this study, we used the Ionospheric Plasma Irregularities (IPIR) dataset. The IPIR dataset uses Electric Field Instrument (EFI) and GPS Receiver (GPSR) instruments; for details about the dataset, see Jin et al. (2022).

3.0 Observation and Methodology

3.1 IPIR Dataset

The IPIR data product of the SWARM constellation was used to study ionospheric plasma blobs over Nigeria. The IPIR dataset is a Level 2 (L2) data product that results from data assimilation and processing of several Swarm L1b and L2 data products. Its objective is to offer a complete dataset that enables the analysis of plasma structuring along all Swarm orbits (Jin et al., 2022). IPIR utilizes several Swarm products, including plasma density derived from EFIx_LP_1B,

Ionospheric Bubble Index (IBI) obtained from IBIxTMS_2F, auroral boundary detection based on field-aligned currents from AOBxFAC_2F, topside-ionosphere total electron content (TEC) derived from TECxTMS_2F, and Polar Cap Products as described by Spicher et al. (2017). The IPIR dataset comprises 29 entries, but only twelve (12) entries that are relevant to this study were used. Table 1 shows the details of the entries used for this study.

Table 1: IPIR Dataset parameters used for this study. Twelve parameters are considered for this study, and their details are shown in the table.

S/N	Name	Description	Unit
1	Timestamp	CDF epoch of the measurement	-
2	Latitude	Position in ITRF – Latitude	degree
3	Longitude	Position in ITRF – Longitude	degree
4	Ne	Electron density, ne; downsampled to 1 Hz	cm^{-3}
5	Background_Ne	Background electron density, ne,b	cm^{-3}
6	Te	Electron temperature, Te; downsampled to 1 Hz	K
7	Grad_Ne_at_20 km	The electron density gradient over 20 km based on 2 Hz data	cm^{-3}/m
8	ROD	Rate Of change of density, dn/dt	cm^{-3}/s
9	delta_Ne10s	Fluctuation amplitudes over the baseline of 10 seconds	cm^{-3}
10	IBI_flag	Plasma Bubble Index, copied from the Level-2 Ionospheric Bubble Index product, IBIxTMS_2F	-
11	Ionosphere_region_flag	Determining the geomagnetic region where the measurement was taken (0: equator, 1: mid-latitudes; 2: auroral oval; 3: polar cap)	-
12	IPIR_index	Determining the level of fluctuations in the ionospheric plasma density	-

According to Jin et al. (2022) the background density is calculated from n_e using a 35th percentile filter of 551 data points, which corresponds to approximately 2,000 km for 2 Hz data at the Swarm orbital speed of ~7.5 km/s. The parameters delta_Ne10s (i.e., Δn_{e10s}) correspond to the amplitudes of plasma fluctuations. They are obtained by subtracting the median filtered value of n_e within Δt = 10s intervals from the actual value of n_e:

$$\Delta n_{eXs}\,(t_i) = n_e(t_i) - \tilde{n}_e\,(t_i)_{Xs}$$

where $\tilde{n}_e\,(t_i)_{Xs}$ is the median-filtered value of n_e at time t_i, which is median-filtered within a X-second interval. These scales correspond to fluctuations at scales smaller than 75 km (Jin et al., 2022).

The IPIR index was derived from the combination of RODI10s and standard deviation of delta_Ne10s (i.e., of Δn_{e10s}) as thus (Jin et al., 2022):

$$IPIR_{ix} = RODI10s \cdot A(n_e)_{10s}$$

where

$$RODI(t) = \sqrt{\frac{1}{N-1}\sum_{t_i=t-\Delta t/2}^{t_i=t+\Delta t/2} |ROD(t_i) - \overline{ROD}|^2}$$

where $\overline{ROD}$ is the mean value of $ROD(t_i)$:

$$\overline{ROD} = \frac{1}{N}\sqrt{\sum_{t_i=t-\Delta t/2}^{t_i=t+\Delta t/2} ROD(t_i)}$$

where $\Delta t = 10\ seconds\ for\ RODI10s\ and\ A(n_e)_{10s}$ is the standard deviation of Δn_{e10s} in a running window of 10 seconds:

$$A(n_e)_{10s}\,(t) = \sqrt{\frac{1}{N-1}\sum_{t_i=t-\Delta t/2}^{t_i=t+\Delta t/2} |\Delta n_{e10s}(t_i) - \overline{\Delta n_{e10s}}|^2}$$

where $\overline{\Delta n_{e10s}}$ is the mean value of $\Delta n_{e10s}(t_i)$ in this interval:

$$\overline{\Delta n_{e10s}} = \frac{1}{N} \sum_{t_i=t-\Delta t/2}^{t_i=t+\Delta t/2} \Delta n_{e10s}(t_i)$$

$RODI10s$ relates to the variability seen in density fluctuations within plasma, characterizing its structure over 10-second intervals. Meanwhile, $A(n_e)_{10s}$ is associated with the absolute amplitudes of fluctuations occurring in 10-second intervals. The interrelation between $A(n_e)_{10s}$ and $RODI10s$ reveals an insignificant correlation for minor scales. When combined, these measures offer valuable insights into the extent of structuring within ionospheric plasma. Notably, high IPIRix values typically coincide with substantial amplitudes in high-frequency fluctuations. The classification of IPIRix index scale with respect to ionospheric plasma density fluctuations falls into three classifications: 1-3 (low), 4-5 (medium), and >6 (high). This scale represents a tenfold difference in IPIRix numerical values. For example, an index value of 1 corresponds to IPIRix values below 10^3 $cm^{-3}s^{-1}cm^{-3}$, index value 2 corresponds to IPIRix values ranging between 10^3 and 10^4 $cm^{-3}s^{-1}cm^{-3}$, index value 3 corresponds to IPIRix values ranging between 10^4 and 10^5 $cm^{-3}s^{-1}cm^{-3}$, and so forth (Jin et al., 2022). Figure 1 shows the trajectory of the SWARM satellite A (in blue) on March 4, 2019, and the magnetic equator (in red).

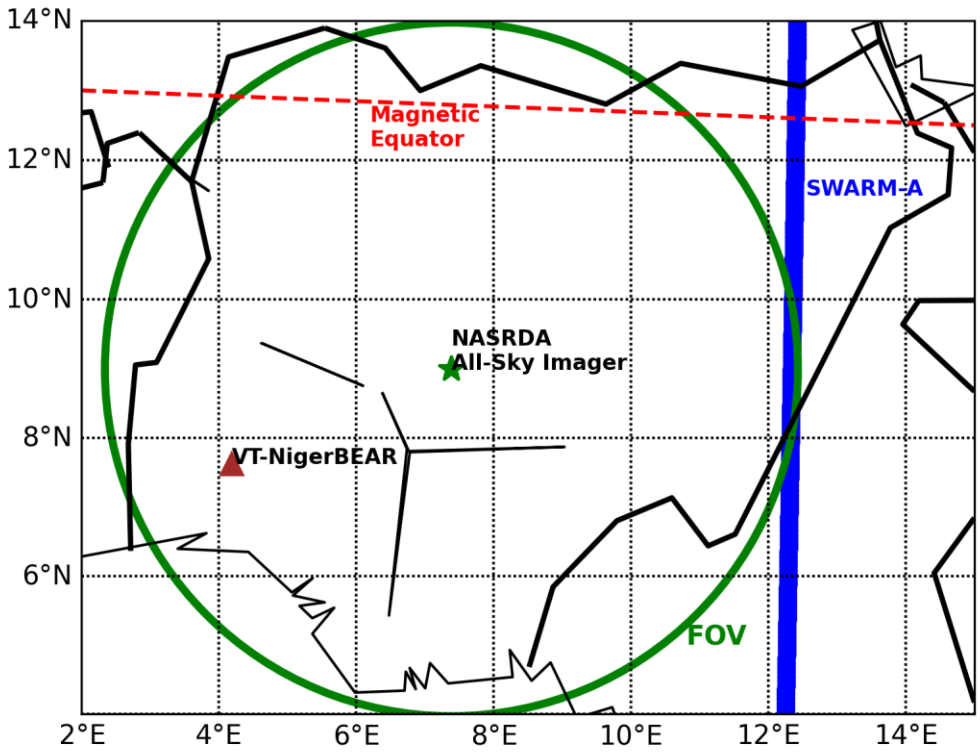

Figure 1: Observatory, All-Sky Imager FOV, SWARM satellite passage, and magnetic equator. The All-Sky Imager is located at SERL-ARCSSTE-E-NASRDA with the field of view (FOV, in green), SWARM satellite passing over Nigeria (in blue), magnetic equator (in red), and the location of the planned Virginia Tech – Nigerian Bowen Equatorial Aeronomy Radar (VT-NigerBear, in planning).

Therefore, in this paper, blobs are identified as discrete regions of enhanced electron density (see Figure 2(a)) while SSFil are identified as continuous irregular fluctuations in the electron density (see Figure 2(b) and (c)). To identify Blob and SSFiI, we conducted a manual search using electron density data, and the other parameters described in Table 1 are used to study their signatures. We established a 5% threshold for plasma density enhancement above the background, meaning that we manually selected blobs when the local electron density increased by more than 5%. SSFiI consists of continuous, irregular fluctuations in electron density with the prominent periods at 2-4 seconds, and there are no corresponding irregular fluctuations observed in the magnetic field data. In cases where there are blobs without SSFil, there are no fluctuations in the electron density (see Figure 2(c) in red and 5(a)). Conversely, when there are blobs with SSFil, continuous electron density fluctuations are present (see Figure 2(b) and (c)). Figure 2(a) illustrates a contour plot of a specific example, depicting a discrete region of enhanced electron density (blob) at 10°N

geographic latitude, located within the trough of the equatorial ionization anomaly (EIA) on March 1, 2019, at 21:52 LT. We visualized 1D electron density data as a 2D filled contour against latitude using the ggplot module of the R programming language (Wickham, 2020) (refer to Figure 5(a) for the line plot of the same data). It's important to note that this plot shows electron density as a function of latitude only, as plotting it against both latitude and longitude would result in a straight contour line due to the satellite's single pass along a longitude, providing little meaningful information. Therefore, we opted for the 'ggplot' module, which allows us to create contour plots with electron density and latitude only. Notably, this blob exhibits a significantly higher concentration (54%) of plasma compared to the background density. Along-track extension of blobs was used to estimate the north-south scale-size of the blobs. This extension was converted to kilometer such as 1° = 110 km. Similar method was also used by Le et al. (2003) to estimate the blobs' extension. In addition, using the Scipy "find_peaks" function, we estimated the wavelength of SSFiI to be 11 km on average. From this parameter, the percentage enhancement of electron density inside the blob as compared to the background density was estimated. Lastly, we estimated the spectral characteristics of SSFiI using discrete Fourier Transform on the electron density data.

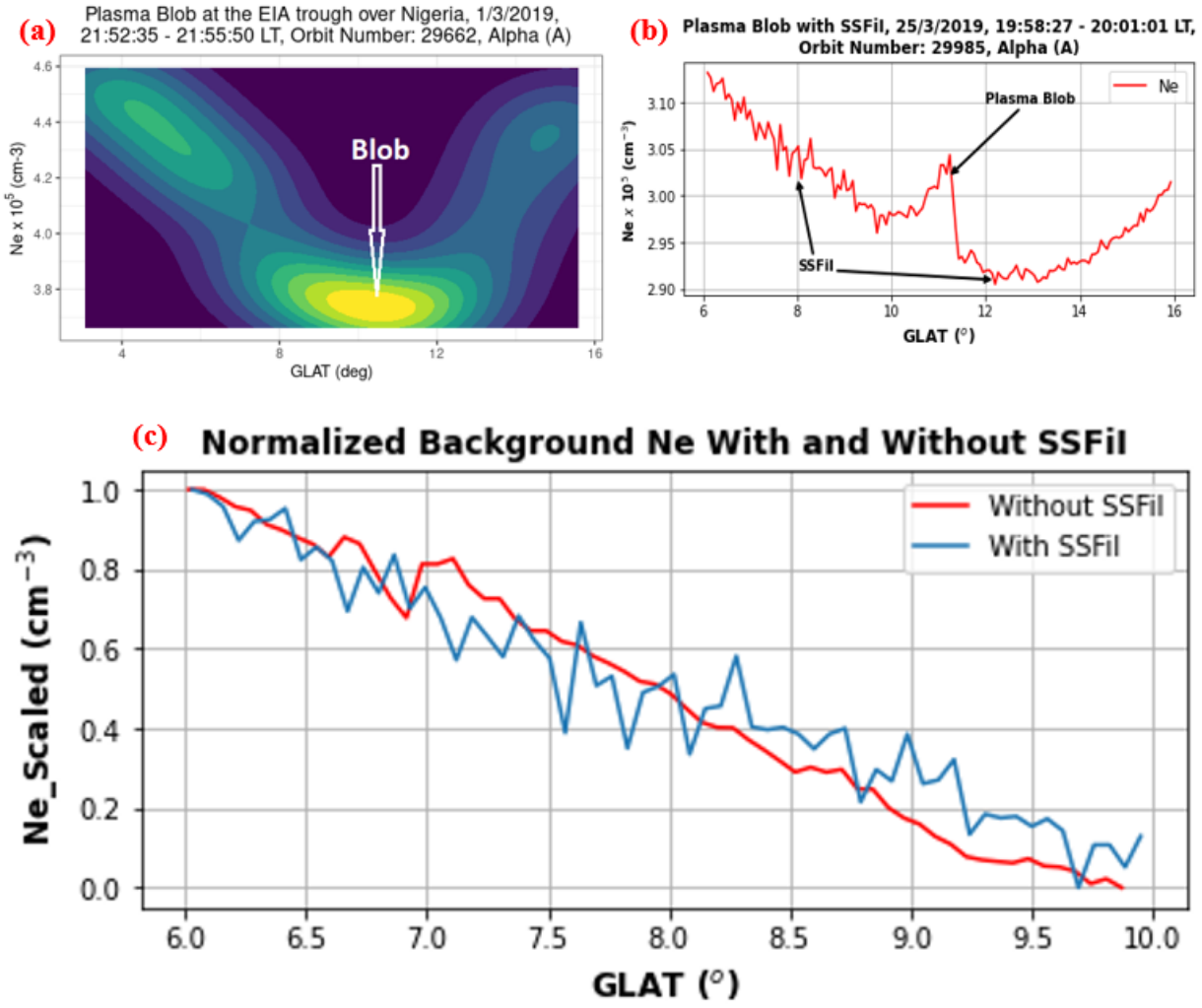

Figure 2: (a) Typical structure of ionospheric plasma blobs (without SSFiI) shown as a discrete enhanced region of electron density located between 8º-12º GLAT. The blob is located at the trough of equatorial ionization anomaly (EIA). The contour plot is a 2D filled visualization of electron density against the latitudes. The similar line plot of the same data is in Figure 5(a). (b) Plasma blob with SSFiI. SSFiI are identified as continuous, irregular fluctuations in the electron density. (c) Background electron density for both cases of blobs with SSFiI (in blue) and blobs without SSFiI (in red).

3.2 Geomagnetic Conditions

With the target to classify the blobs by the geomagnetic conditions using Dst values, Figure 3 shows the Dst values for each case in 2019. Blobs have been observed during geomagnetic storms, Dst < -50 nT (Pimenta et al., 2007) and quiet geomagnetic conditions, Dst > -50 nT (Park et al., 2022). Following the geomagnetic storm classification of Gonzalez et al. (1994) none of the

observed 41 cases was related to geomagnetic storms because the Dst values were typically greater than -50 nT (see Figure 3). This implies that the influence of prompt penetration of the electric field of the higher latitude origin is ruled out as the possible cause of these blobs.

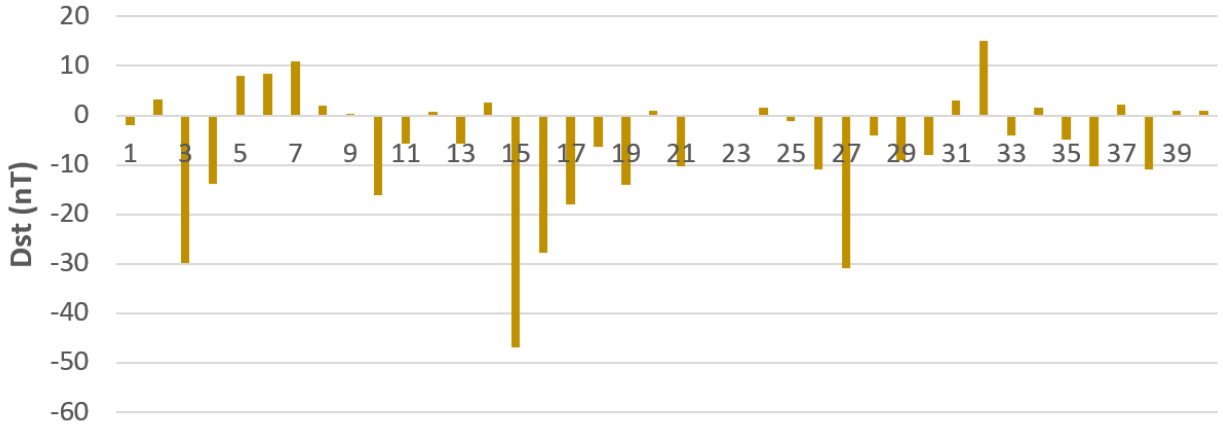

Figure 3: Dst values for each of the 41 cases of blobs over Nigeria. The Dst data was obtained from VirEs of the SWARM mission.

4.0 Results and Discussion

4.1 Occurrence patterns

We have analyzed the 2019 Swarm data via the Virtual Research Environment (VirEs) of the SWARM constellation mission (Smith et al., 2022). For 2019, the satellites passed over Nigeria 126 times with 41 cases of plasma blobs, see Figure 4 for the distribution of the cases. Three clusters of cases can be observed: January through March, June through August, and October through December. August has the highest occurrence rate (77%) of blobs. There is a 17% occurrence rate of plasma blobs during solstices (June and December), and 10% occurrence rate during March equinox with no case in September equinox. Dividing the occurrences into local summer (April to October) and winter (November to March) seasons in Nigeria, there are 22 cases (54%) in summer and 19 cases in winter (46%). Thus, there seems to be more cases in summer than in winter. This is opposite to the blobs' seasonal distribution, as Park et al. (2008) reported, where most of the blobs occurred during winter. Su et al. (2022) also conducted a statistical study on the occurrence characteristics of plasma blobs. They found that the seasonal pattern peaks in June Solstice in both the northern and southern hemispheres, opposite to what has been observed

in this study. However, the blobs' occurrence patterns over Brazil carried out by Adebayo (2021) showed zero occurrences in April, May and June, which is similar to the results in the current study. The similarity between these studies could be a result of the proximity of the two observatories (Brazil and Nigeria) to the equatorial region than the other studies with opposite results, which probably suggests that there are variety of plasma blobs and, thus, various mechanisms for their development and morphology.

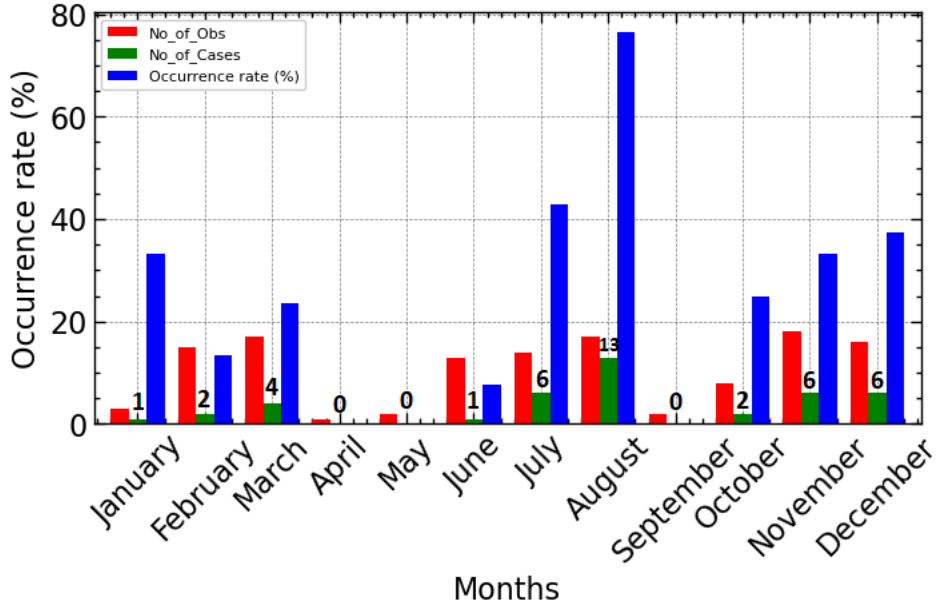

Figure 4: Occurrence patterns of plasma blobs over Nigeria in 2019. The red bars show the observation which correspond to the number of times the satellites passed over Nigeria in 2019, and the green bars show the number of cases of blobs for each month.

However, from the distribution pattern of the observations (red bars in Figure 4), it can be observed that some of the months have very few or no observations at all, which implies the absence of satellites passing over Nigeria in that period due to the 1800 – 0459 (LT) time constraints. Thus, the results obtained for April, May and September may not be reliable indicators of the blob's actual percentage of occurrence in nature. This is because the limited number of satellites passes during these months results in a small sample size, which may not be representative of the entire population. As a result, the computed percentage occurrence (in blue) may be subject to significant sampling error and may not accurately reflect the blob's true occurrence in nature. Thus, this makes

it difficult to draw reliable conclusions about seasonal patterns in the blob's occurrence over Nigeria.

From Figure 5, selected cases of blobs over Nigeria shown as discrete enhanced regions of electron density can be seen at around 10ºN geographic latitude. The figure shows the presence of small-scale fluctuations in ionospheric (SSFiI) plasma density (seen as irregular fluctuations in Figure 5 (b), (c), and (d)). The signatures of the blobs associated with SSFil differ from those without SSFiI (to be discussed in the subsequent sections). We observed that the blobs associated with SSFiI shrank with north-south extension being smaller by ~62% (on average) than the blobs without SSFiI. In addition, the plasma within the blobs associated with SSFiI are more disturbed with clearer evidence of the presence of medium-scale irregularities when compared with their counterpart. The rate of change of the electron density inside the blobs associated with small-scale fluctuations was ~50% above that of the blobs without. The SSFiI might have been induced by the atmospheric gravity waves or due to the plasma instability in the ionosphere itself. However, there is no clear explanation for the main course of these SSFiI. Further research is therefore required to identify the source and dynamics of these SSFiI in the ionosphere.

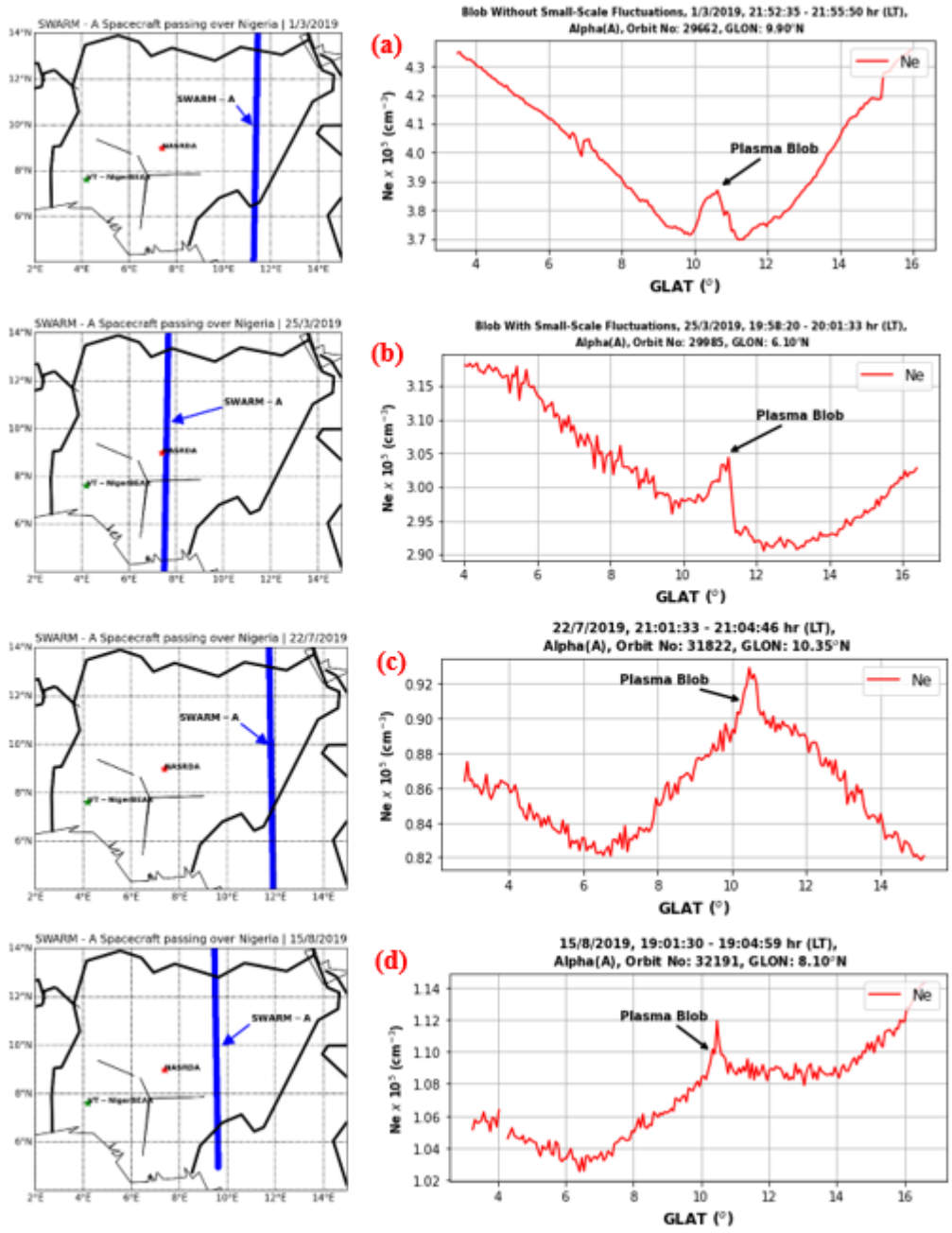

Figure 5: Samples of plasma blobs observed over Nigeria. The red line in the right-side plots is the electron density, with obvious fluctuations in (b), (c), and (d), and none of such in (a). These fluctuations are the small-scale variations in the ionosphere plasma density. The blue line in the left-side plots indicates the trajectory of SWARM A over Nigeria.

247

248

249

4.2 Spectral Analysis of SSFiI

The spectral analysis of SSFiI using discrete Fourier Transform method is shown in Figure 6 where the results are visualized in terms of the magnitude spectrum, and periodogram. Note that only one side of the spectrum is considered in the figures. The magnitude spectrum illustrates an exponential decrease in the magnitude of SSFiI with increasing frequency, revealing fluctuations in magnitude occurring shortly after approximately 0.25 Hz. The periodogram shows that the most significant frequencies of SSFiI have periods of approximately less than 6.5 seconds (the red vertical line). The position of the red vertical line in the periodogram signifies the boundary between the considered and the cut-off frequencies. This is because the cluster of the magnitude/frequency bins lies mostly at periods less than 6.5 seconds. So, the main peaks residing at periods less than 6.5 seconds are considered as the most occurring periods and thus, the prominent frequencies. Hence, SSFiI have periods of 2-4 seconds and propagating at the speed of 2.75 – 5.5 km/s using the 11 km (along-track extension) average wavelength.

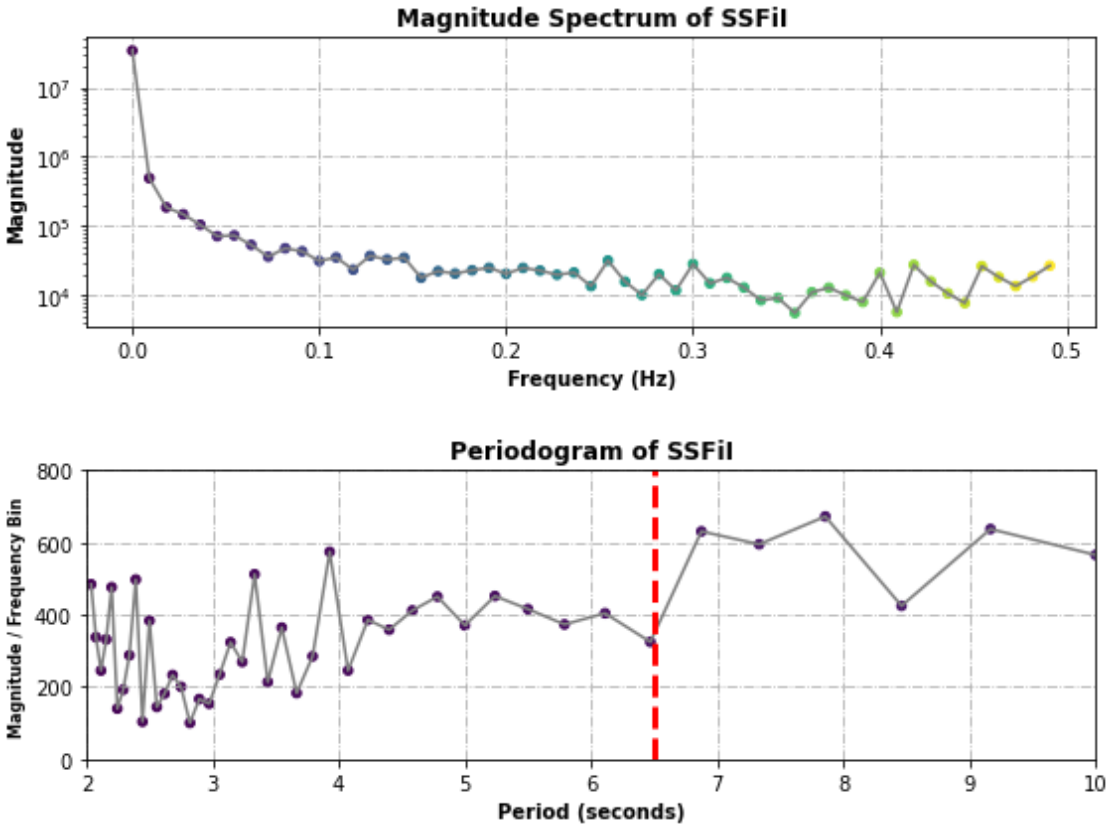

Figure 6: Spectral analysis of SSFiI: Top panel shows the magnitude spectrum of SSFiI, second panel shows the periodogram of SSFiI. The red vertical line in the periodogram indicates the considered and the cut-off frequencies.

4.2 Signatures of Ionospheric Plasma Blobs

With the target to evaluate the signatures of blobs in the topside ionosphere over Nigeria, we have selected two prominent cases within which the 41 cases are classified visually: cases without SSFiI and with SSFiI. In other words, each of the cases observed demonstrates one of these signatures, excluding the blobs associated with bubbles. We are not focusing on the blobs associated with bubbles in this study as several investigators have already reported such (Park et al., 2022b, Su et al., 2022; Agyei-Yeboah et al., 2021; Wang et al. 2019). The signatures of the blobs are studied on the parameters highlighted in Table 1. The hatched region is approximately just showing the electron density enhancement and the corresponding signatures on the parameters. But notice that some parameters show different structures even beyond the hatched region such as the latitudinal variations.

4.2.1 First Case Study – Without SSFiI

From the first case study, Figure 7(a), which is without the presence of small-scale fluctuations, the electron density inside the blob increased significantly above the ambient density (panel (a)); the electron temperature fluctuates inside the blob with a sinusoidal pattern (panel (b)), the ionospheric plasma irregularities index (panel (d)) does not show precise pattern at the exact location of the blobs however, there is a jump of IPIRix from 3 to 4 level at around the location of the blob. The electron density gradient at 20 km (panel (e)) displays an initial decrease in electron density and sudden increase inside the blob, plasma fluctuation amplitude over the 10s baseline (panel (f)) display slight increase in turbulence inside blob, and the rate of change of electron density (panel (g)) increases significantly inside the blob. The gradient of electron density at 20 km (e) and rate of change of electron density (g) display similar patterns: the gradient is positive southward of the blob (from 2ºN to 10ºN GLAT), abrupt increase inside the blobs, then negative northward of the blobs (from 12 ºN to 16ºN GLAT). A recovery pattern can be seen at the northward of the blobs as the gradient approaches “0” (see Figure 7(e) and (g)). This result is similar and in agreement with the plasma drifts behavior inside the blobs as reported by Klenzing et al. (2011) and Le et al. (2003). In their work, they attributed the reversal to the evening-to-night electric field reversal. Thus, it can be inferred that blobs are likely harboring small-medium scale irregularities which could pose abnormality on the radio signal passing through or around them.

Wang et al. (2015) reported a case of scintillation associated with ionospheric plasma blobs, and they found that plasma was greatly disturbed inside the blob. Shi et al. (2017) also reported that ionospheric plasma blobs could cause scintillation as the plasma was greatly disturbed inside the blobs. Watanabe and Oya (1986) reported a significant increase in electron density inside the blobs. According to a study by Park et al. (2003), the electron temperature within the blobs was found to be lower, and the ratio of O^+ to H^+ ions was greater than that of ambient plasma. They suggested that plasma blobs originate from the lower part of F region. Thus, this work agrees with the earlier reported signatures of blobs.

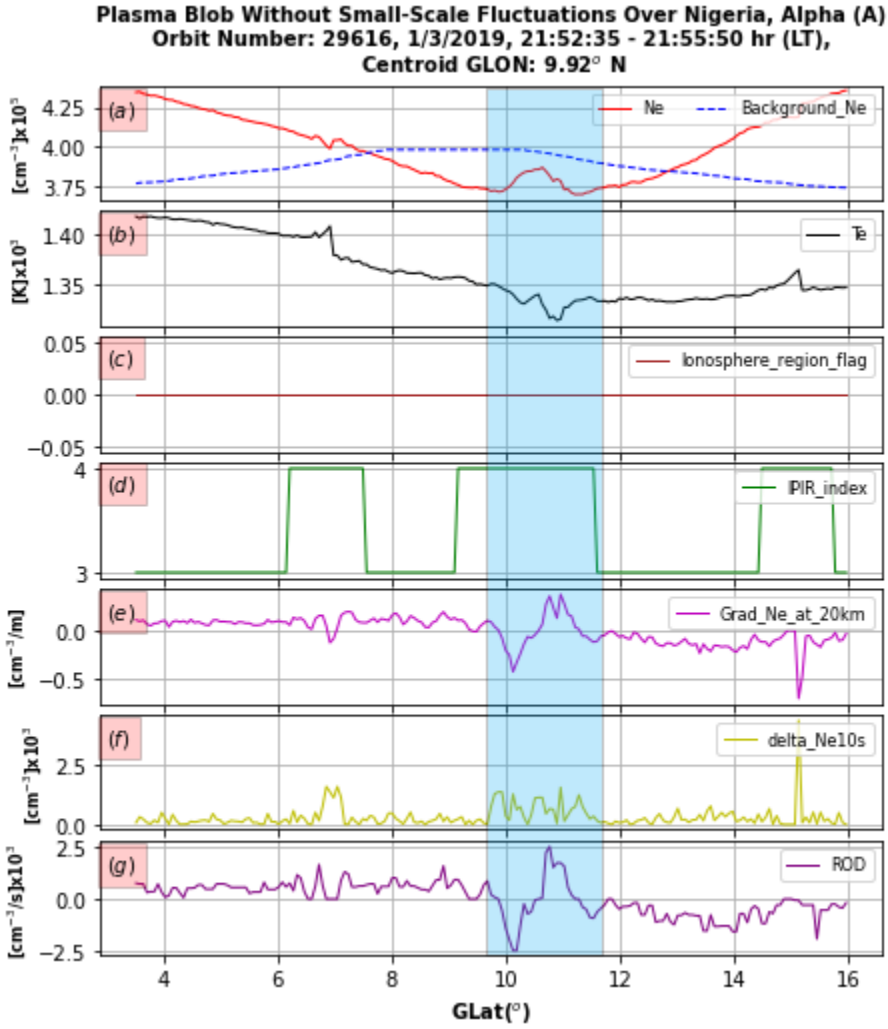

Figure 7: First classification of the signature of plasma blobs without the presence of small-scale fluctuations in ionosphere plasma density. The greyed section shows the region of the blob and corresponding signatures.

4.2.2 Second Case Study – With SSFiI

Figure 8 shows a plasma blob in the presence of small-scale fluctuations in ionosphere plasma density. In comparison to Figure 7, notable differences can be observed in the signatures of the blobs associated with SSFiI and those without. The electron density (panel (a)) increased significantly inside the blob (similar to the first case study), the electron temperature (panel (b)) does not show a precise pattern however, a sudden increase in the temperature (25% above the ambient temperature) between 8.5ºN and 14ºN can be observed, with a sharp drop at the blob's centroid. The IPIR index indicates more precisely that there are irregularities in the blob's temperature, density, or its thermal characteristics, as seen by the IPIR index suddenly and very precisely jumped from 2 to 4 scale (see Figure 8(d)). The poleward edges of the blobs are more relatively stable when compared within the blobs. The electron density gradient at 20 km (panel (e)), plasma fluctuation amplitudes on 10s baseline (panel (f)), and the rate of change of electron density (panel (g)) glaringly show that these blobs display different signatures compared to the blobs without SSFiI. The rate of change of the electron density inside the blobs associated with SSFiI was ~50% above that of the blobs without. The distinctive features of these plasma blobs encompass a notable increase in electron plasma density, a solely positive electron gradient within the blob see Figure 8(e), (f) and (g), and a substantial increase in the amplitude of plasma fluctuation. In comparison to the initial scenario, it can be deduced that the presence of SSFiI is linked to significant perturbations within the plasma blobs. Considering the non-stationary property of these small-scale fluctuations, probably induced by atmospheric gravity waves originating from lower altitudes (Takahashi et al., 2022; Suzuki et al., 2008) or by instabilities in the ionosphere itself, these fluctuations might have propagated towards the equator and interacted with ionospheric plasma blobs. This interaction could have transferred momentum and energy to the plasma blobs, causing larger irregularities and turbulence within them, which we can observe when studying these plasma blobs associated with small-scale plasma fluctuations.

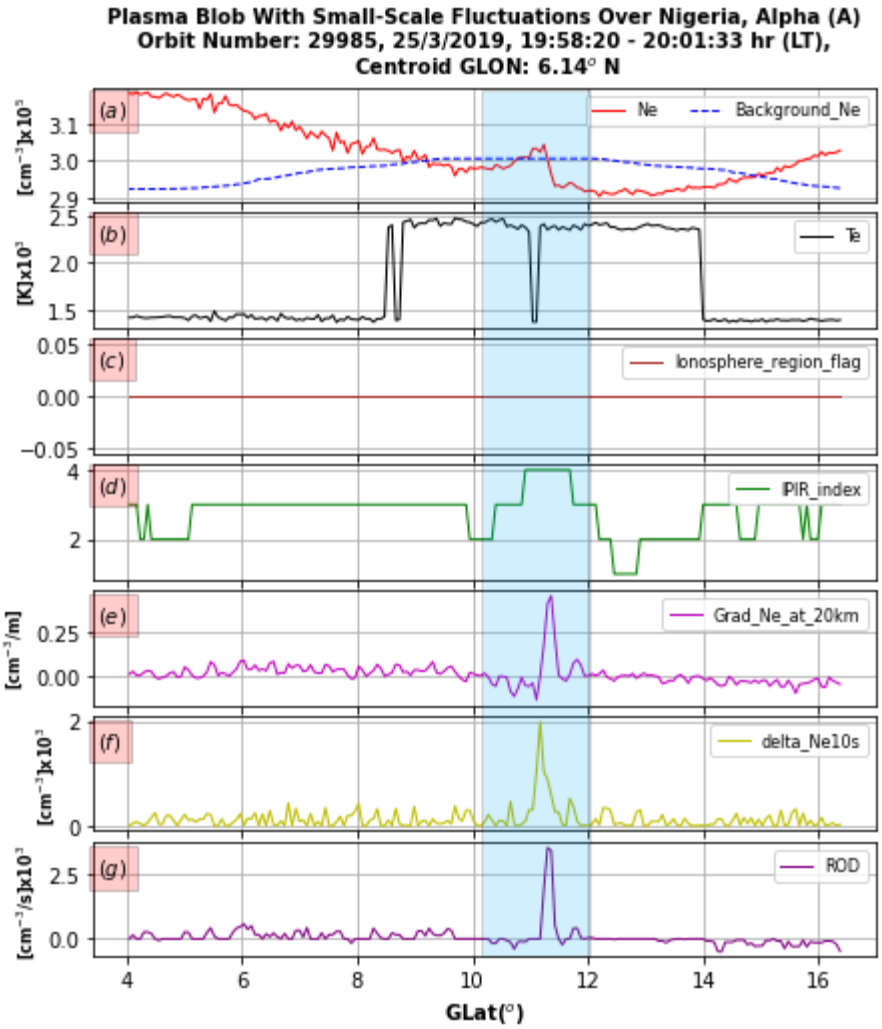

Figure 8: Second case of plasma blobs but in the presence of small-scale fluctuations in the ionosphere plasma density.

Exploring the potential impact of SSFiI, this investigation unveils characteristic plasma behavior within the context of plasma blobs associated with SSFiI. In Figure 9, we present electron density, IPIR_index, and plasma fluctuation amplitude within three selected blob cases. The IPIR_index exhibited a transition from a low-level plasma fluctuation (2) in the immediate surroundings to a medium level (4) within the blob across all cases. This suggests a heightened degree of plasma turbulence within the blob compared to its immediate surroundings, a pattern affirmed by the amplitude of plasma fluctuation (depicted in yellow). Notably, the amplitude of plasma fluctuation is substantially higher within the blobs, showing an average percentage increase of 290% relative to blobs without SSFiI. In contrast, blob events in the absence of SSFiI lack such a uniform

distinctly increased level of plasma turbulence (see Figure 7(f)). Thus, the presence of SSFiI introduces an additional layer of plasma irregularity to blobs, potentially exerting influences on radio wave technologies.

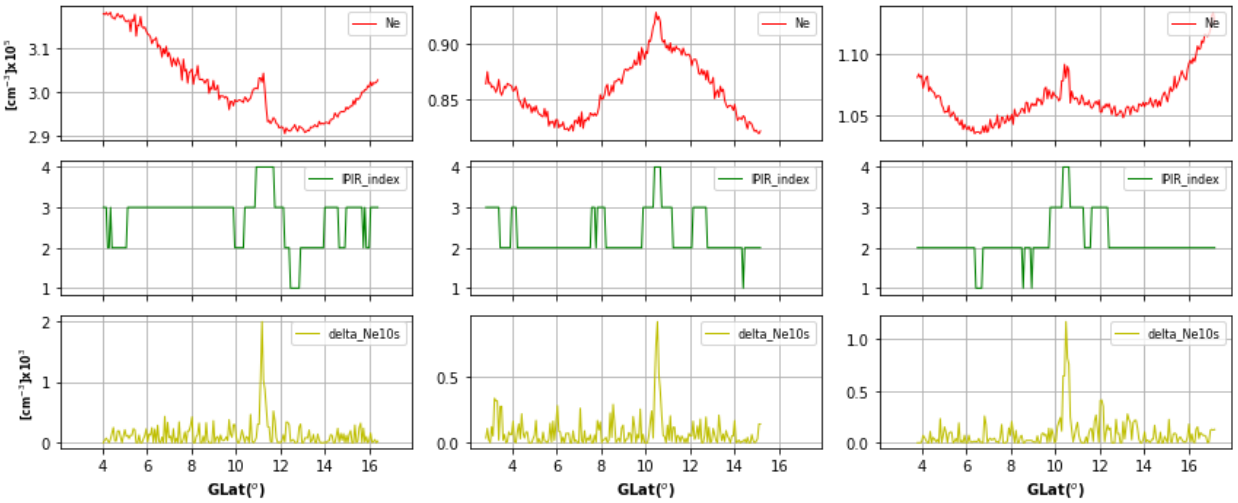

Figure 9: Uniform patterns observed for the blobs associated with SSFiI. The fist panel (in red) shows the electron density, the second panel (in green) shows the IPIR_index, and the third panel shows the plasma amplitude fluctuation.

4.3 Statistical analysis of Plasma Blobs

To further understand the physical characteristics of the blobs observed over Nigeria, statistical analysis has been performed on the key features of the blobs, and this includes number of cases (No_of_Cases), average electron density (Density (cm^{-3})), average north-south extension of the blobs (N-S Extension (km)), average geographical latitudes (GLAT (º)), average geographical longitude (GLON (º)), see Table 2. The average values are based on the monthly cases of the blobs. The blobs have a north-south extension of 46.62 – 182.04 km (approximately 107.97 ± 31.81 km on average), an average electron density of 2.29×10^5 cm^{-3} and an average latitude (longitude) of 10.62 ± 0.32º (10.43 ± 4.08). Figure 10 shows the frequency distribution of the north-south scale size of the blobs observed over Nigeria in 2019. 66% of the cases are less than 120 km in north-south extension. Adebayo (2021), using optical instruments, estimated the north-south and east-west extensions of blobs during low solar activity as 110-230 km and 41-81 km, respectively. Pimenta et al. (2007) reported the scale sizes of blobs during geomagnetic storms to be 200-460 km and 110-160 km in north-south and east-west extensions, respectively. Therefore, considering

360 the range of values obtained in this study it can be inferred that the results agree with the previous
361 studies.
362
363 *Table 2: Blobs statistical parameters monthly. The average of each of the cases is summarized in*
364 *the table.*

Months	**No_of _Obs**	**No_of_ Cases**	**Occurrence (%)**	**Density (10^5 cm^{-3})**	**N-S Extension (km)**	**GLAT (º)**	**GLON (º)**
January	3	1	33.3	0.987	132.10	10.45	15.35
February	15	2	13.3	2.501	77.70	10.38	15.13
March	17	4	23.5	3.432	129.32	10.82	10.19
April	1	0	0.0	-	-	-	-
May	2	0	0.0	-	-	-	-
June	13	1	7.7	2.094	57.72	10.87	5.54
July	14	6	42.9	1.796	93.06	10.76	8.06
August	17	13	76.5	2.331	107.58	10.74	8.90
September	2	0	0.0	-	-	-	-
October	8	2	25.0	2.229	112.11	10.57	9.42
November	18	6	33.3	2.374	120.62	10.28	12.61
December	16	6	37.5	2.103	94.54	10.47	13.66

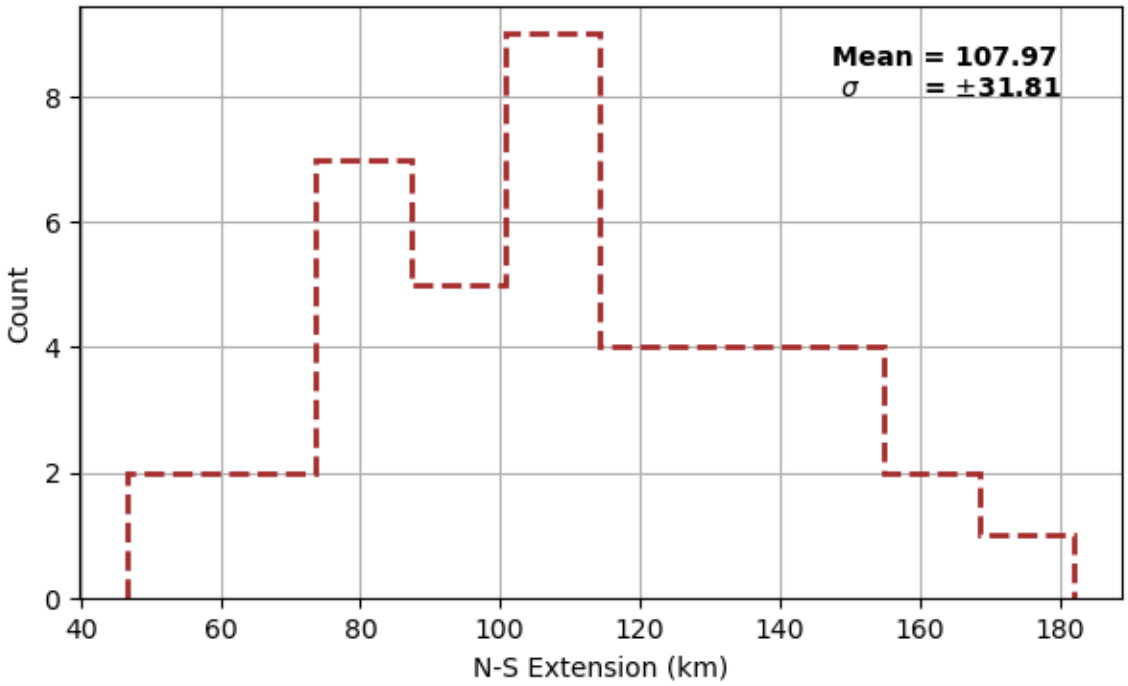

Figure 10 Distribution of north-south extension of the blobs over Nigeria in 2019. The blobs are 107.97 km on average with minimum and maximum scale size of 46.62 – 182.04 km, respectively.

5.0 Conclusions

Plasma blobs are localized enhanced regions of plasma above ambient plasma. Since the first observation of plasma blobs by Watanabe and Oya (1986), there has been a series of research investigating the origin, dynamics, and morphology of plasma blobs across different regions of the globe. Plasma blobs are not phenomena exclusively occurring in the ionosphere; they have also been observed in other plasma forms. Thus, understanding the physics of blobs is very crucial.

In this study, we have observed ionospheric plasma blobs over Nigeria with the ESA SWARM satellites using the ionospheric plasma irregularities dataset. This work signifies the first occurrence characteristics of plasma blobs over Africa and the possible influence of small-scale plasma fluctuations in the ionospheric plasma density. We couldn't affirm the actual occurrence patterns of blobs over Nigeria due to the sampling error in the observation and cases statistics of

379 blobs. We imposed a time frame of 1800 – 0459 LT on the satellite observations over Nigeria so
380 as to study only the nighttime blobs. However, likely relevant information to the literature was
381 deduced. The signatures of plasma blobs have been classified into two categories: with small-scale
382 fluctuations in ionosphere (SSFiI) plasma density and without these fluctuations. From the spectral
383 analysis, SSFiI have periods of 2-4 seconds and propagating at the speed of 2.75 – 5.5 km/s using
384 the 11 km (along-track extension) average wavelength. The result shows that plasma inside the
385 blobs associated with SSFiI is more disturbed than the ones without these fluctuations. SSFiI could
386 be responsible for this increased disturbance. Plasma density fluctuations are frequent occurrence
387 in the ionosphere and can be caused by many factors such as atmospheric gravity waves activities
388 (Hocke and Tsuda, 2001), high latitude plasma dynamics (Chaturvedi, 1976), geomagnetic storms
389 (Takahashi et al., 2018), passing of very low frequency signal transmitter (Ivarsen et al., 2021) to
390 mention a few. These fluctuations can initiate various plasma irregularities phenomena whose
391 presence could pose significant impacts on ground-based and space-based technologies. In this
392 study, we have found that blobs were greatly disturbed by the presence of small-scale fluctuations
393 in plasma density with the evidence of higher amplitude of plasma fluctuation, and this support
394 the earlier results of blobs' potential to causing scintillation (Shi et al., 2017; Wang et al., 2015).
395 However, the source of SSFiI couldn't be affirmed in this work and thus, further investigation is
396 required.
397
398 The blobs were mostly found at the crests and troughs of equatorial ionization anomaly which is
399 quite similar to other reported blobs (Luo et al., 2018; Park et al., 2022). The blobs associated with
400 plasma bubbles may be explained by the hypothesis proposed by Huang et al. (2014) where blobs
401 development has been linked to bubbles evolution. However, Adebayo (2021) found cases of
402 bubbles without blobs over the Brazilian sector using optical instruments, and they inferred that
403 polarized electric field might be the key driver of the formation of plasma blobs associated with
404 bubbles. They concluded that there might be a threshold of polarized electric field liable for blobs'
405 development as the cases of bubbles without blobs showed a relatively shorter depletions when
406 compared with bubbles associated with blobs. In this paper, the blobs found at the crests of EIA
407 and in the absence of bubbles are more likely to be caused by the mechanisms simulated by Krall
408 et al. (2010) where blobs are formed at the balance of upward diffusive force and downward
409 gravitational and pressure gradient forces. But the simulation did not show formation of blobs at

the trough of EIA neither has there been any observation of such, thus, the blobs found in the absence of bubbles and at the trough of EIA in this study are probably generated by the nonuniform behavior of Pedersen current induced by the thermospheric neutral wind. However, further investigations on the physics of these blobs are important to validate these hypotheses.

In summary, this study observed only a few numbers of cases where blobs were found to be associated with bubbles, suggesting that the presence of bubbles alone may not be sufficient for the development of blobs. Furthermore, the observation of plasma blobs associated with small-scale fluctuations in ionosphere plasma density suggests that there may be additional mechanisms at work, independent of bubbles, that contribute to the formation and dynamics of plasma blobs. In addition, it is noteworthy that none of the observed blobs associated with small-scale fluctuations occurred in the presence of bubbles. Thus, suggesting that the physical processes underlying the formation of plasma blobs may differ from those involved in the formation of bubbles. Nevertheless, the exact mechanisms underlying the interaction between small-scale fluctuations and ionospheric plasma blobs are still an active area of research; hence, further simulations exploring the mechanisms proposed earlier by other investigators may provide insights into the dominant mechanisms that give rise to plasma blobs.

Acknowledgements

We would like to express our heartfelt gratitude to several individuals and organizations who played pivotal roles in making this research possible. First and foremost, we extend our sincere appreciation to the Federal Government of Nigeria, channeled through the United Nations African Regional Centre for Space Science and Technology Education of the National Space Research and Development Agency (NASRDA), for their financial support. Additionally, we acknowledge the European Space Agency (ESA) for generously providing access to satellite data crucial for our research. Furthermore, we recognize the significant contribution of Ashley Smith, whose Python tools greatly facilitated the retrieval and analysis of swarm data. Oluwasegun Adebayo appreciates the constructive criticism from the professors. Their feedback played a pivotal role in enhancing the quality of this manuscript. Lastly, we would like to acknowledge the support received from the Japan Society for the Promotion of Science, Japan, under grants 15H05815, 16H06286, 21H04518, and JPJSCCB20210003.

Open Research

The satellite data used for this research can be freely obtained from https://earth.esa.int/web/guest/swarm/data-access. The python code for the data analysis and visualization is made available on GitHub.

References

Adebayo, M. O., Pimenta, A. A., Savio, S., & Nyassor, P. K. (2023). Airglow Imaging Observations of Plasma Blobs: Merging and Bifurcation during Solar Minimum over Tropical Region. *Atmosphere, 14*(3), 514.

Adebayo, M. O. (2021, November 18). *Plasma blobs in the tropical region: A study using ground-based optical and radio techniques and multisatellite data*. Redirection to the Bibliographic Mirror. Retrieved March 21, 2023, from http://mtc-m21d.sid.inpe.br/col/sid.inpe.br/mtc-m21d/2021/07.19.19.39/doc/thisInformationItemHomePage.html

Agyei-Yeboah, E., Fagundes, P. R., Tardelli, A., Pillat, V. G., Pignalberi, A., Kavutarapu, V., Pezzopane, M., & Vieira, F. (2021). Ground and satellite-based observations of ionospheric plasma bubbles and blobs at 5.65° latitude in the Brazilian sector. *Advances in Space Research, 67*(8), 2416–2438.

Chaturvedi, P. K. (1976). Collisional ion cyclotron waves in the auroral ionosphere. *Journal of Geophysical Research, 81*(34), 6169-6171.

De Keyser, J., Darrouzet, R., Roth, M., Vaisberg, O., Rybjeva, N., Smirnov, V., Avanov, L., Nemecek, Z., & Safrankova, J. (2001). Transients at the dusk side magnetospheric boundary: Surface waves or isolated plasma blobs? *Journal of Geophysical Research: Space Physics*, *106*(A11), 25503–25516.

Fejer, B., Kudeki, E., & Farley, D. (1985). Equatorial F region zonal plasma drifts. *Journal of Geophysical Research: Space Physics*, *90*(A12), 12249–12255.

Gonzalez, W., Joselyn, J.-A., Kamide, Y., Kroehl, H. W., Rostoker, G., Tsurutani, B., & Vasyliunas, V. (1994). What is a geomagnetic storm? *Journal of Geophysical Research: Space Physics*, *99*(A4), 5771–5792.

Haaser, R., Earle, G., Heelis, R., Klenzing, J., Stoneback, R., Coley, W., & Burrell, A. (2012). Characteristics of low-latitude ionospheric depletions and enhancements during solar minimum. *Journal of Geophysical Research: Space Physics*, *117*(A10).

Hocke, K., & Tsuda, T. (2001). Gravity waves and ionospheric irregularities over tropical convection zones observed by GPS/MET radio occultation. *Geophysical Research Letters*, *28*(14), 2815-2818.

Huang, C., Le, G., de La Beaujardiere, O., Roddy, P., Hunton, D., Pfaff, R., & Hairston, M. (2014). Relationship between plasma bubbles and density enhancements: Observations and interpretation. *Journal of Geophysical Research: Space Physics*, *119*(2), 1325–1336.

Ivarsen, M. F., Park, J., Jin, Y., & Clausen, L. B. (2021). Ionospheric plasma fluctuations induced by the NWC very low frequency signal transmitter. *Journal of Geophysical Research: Space Physics*, *126*(5), e2021JA029213.

Jin, Y., Kotova, D., Xiong, C., Brask, S. M., Clausen, L. B., Kervalishvili, G., Stolle, C., & Miloch, W. J. (2022). Ionospheric Plasma IRregularities-IPIR-data product based on data from the Swarm satellites. *Journal of Geophysical Research: Space Physics*, *127*(4), e2021JA030183.

Kelley, M. C. (2009). *The Earth's ionosphere: Plasma physics and electrodynamics*. Academic press.

Kil, H., Paxton, L. J., Jee, G., & Nikoukar, R. (2019). Plasma blobs associated with medium-scale traveling ionospheric disturbances. *Geophysical Research Letters*, *46*(7), 3575–3581.

Klenzing, J., Rowland, D., Pfaff, R., Le, G., Freudenreich, H., Haaser, R., Burrell, A., Stoneback, R., Coley, W., & Heelis, R. (2011). Observations of low-latitude plasma density enhancements and their associated plasma drifts. *Journal of Geophysical Research: Space Physics*, *116*(A9).

Krall, J., Huba, J., Joyce, G., & Yokoyama, T. (2010). *Density enhancements associated with equatorial spread F*. *28*(2), 327–337.

Luo, W., Xiong, C., Zhu, Z., & Mei, X. (2018). Onset condition of plasma density enhancements: A case study for the effects of meridional wind during 17–18 August 2003. *Journal of Geophysical Research: Space Physics*, *123*(8), 6714-6726.

Le, G., Huang, C., Pfaff, R., Su, S., Yeh, H., Heelis, R., Rich, F., & Hairston, M. (2003). Plasma density enhancements associated with equatorial spread F: ROCSAT-1 and DMSP observations. *Journal of Geophysical Research: Space Physics*, *108*(A8).

Majeski, S., Ji, H., Jara-Almonte, J., & Yoo, J. (2021). Guide field effects on the distribution of plasmoids in multiple scale reconnection. *Physics of Plasmas*, *28*(9), 092106.

Miller, E., Kil, H., Makela, J., Heelis, R., Talaat, E., & Gross, A. (2014). *Topside signature of medium-scale traveling ionospheric disturbances*. *32*(8), 959–965.

505 Okoh, D., Rabiu, B., Shiokawa, K., Otsuka, Y., Segun, B., Falayi, E., Onwuneme, S., & Kaka, R.
506 (2017). First Study on the Occurrence Frequency of Equatorial Plasma Bubbles over
507 West Africa Using an All-Sky Airglow Imager and GNSS Receivers. *Journal of*
508 *Geophysical Research: Space Physics*, *122*(12), 12–430.
509 Park, J., Huang, C., Eastes, R. W., & Coster, A. J. (2022). Temporal Evolution of Low-Latitude
510 Plasma Blobs Identified From Multiple Measurements: ICON, GOLD, and Madrigal
511 TEC. *Journal of Geophysical Research: Space Physics*, *127*(3), e2021JA029992.
512 Park, J., Min, K. W., Eastes, R. W., Chao, C. K., Kim, H.-E., Lee, J., Sohn, J., Ryu, K., Seo, H.,
513 & Yoo, J.-H. (2022). Low-latitude plasma blobs above Africa: Exploiting GOLD and
514 multi-satellite in situ measurements. *Advances in Space Research*.
515 Park, J., Heelis, R., & Chao, C. K. (2021). Ion velocity and temperature variation around topside
516 nighttime irregularities: Contrast between low-and mid-latitude regions. *Journal of*
517 *Geophysical Research: Space Physics*, *126*(2), e2020JA028810.
518 Park, J., Min, K. W., Lee, J., Kil, H., Kim, V. P., Kim, H., Lee, E., & Lee, D. Y. (2003). Plasma
519 blob events observed by KOMPSAT-1 and DMSP F15 in the low latitude nighttime
520 upper ionosphere. *Geophysical Research Letters*, *30*(21).
521 Park, J., Stolle, C., Lühr, H., Rother, M., Su, S. Y., Min, K. W., & Lee, J. J. (2008). Magnetic
522 signatures and conjugate features of low-latitude plasma blobs as observed by the
523 CHAMP satellite. *Journal of Geophysical Research: Space Physics*, *113*(A9).
524 Pimenta, A., Sahai, Y., Bittencourt, J., & Rich, F. (2007). Ionospheric plasma blobs observed by
525 OI 630 nm all-sky imaging in the Brazilian tropical sector during the major geomagnetic
526 storm of April 6–7, 2000. *Geophysical Research Letters*, *34*(2).
527 Shi, J., Wang, Z., Torkar, K., Zherebtsov, G., Ratovsky, K., & Nomanova, E. (2017). *Study on*
528 *plasma blob to result in radio signal scintillations in low latitude ionosphere*. 2004–
529 2007.
530 Shiokawa, K., Katoh, Y., Satoh, M., Ejiri, M. K., Ogawa, T., Nakamura, T., ... & Wiens, R. H.
531 (1999). Development of optical mesosphere thermosphere imagers (OMTI). *Earth,*
532 *Planets and Space*, *51*, 887-896.
533 Shiokawa, K., Otsuka, Y., & Ogawa, T. (2009). Propagation characteristics of nighttime
534 mesospheric and thermospheric waves observed by optical mesosphere thermosphere
535 imagers at middle and low latitudes. *Earth, planets and space*, *61*, 479-491.

536 Smith, A. R. A., Pačes, M., & Swarm, D. I. S. C. (2022). Python tools for ESA's Swarm
537 mission: VirES for Swarm and surrounding ecosystem. *Frontiers in Astronomy and*
538 *Space Sciences*, *9*, 1002697.
539 Spicher, A., Cameron, T., Grono, E., Yakymenko, K., Buchert, S. C., Clausen, L. B. N.,
540 Knudsen, D. J., McWilliams, K. A., & Moen, J. I. (2015). Observation of polar cap
541 patches and calculation of gradient drift instability growth times: A Swarm case study.
542 *Geophysical Research Letters*, *42*(2), 201–206.
543 Spicher, A., Clausen, L. B. N., Miloch, W. J., Lofstad, V., Jin, Y., & Moen, J. I. (2017).
544 Interhemispheric study of polar cap patch occurrence based on Swarm in situ data.
545 *Journal of Geophysical Research: Space Physics*, *122*(3), 3837–3851.
546 Su, S.-Y., Shih, Y.-J., Chao, C.-K., Tsai, L.-C., & Liu, C. (2022). A statistical study on the
547 occurrence characteristics of low-to-midlatitude ionospheric density enhancements
548 (plasma blobs). *Advances in Space Research*, *69*(8), 2957–2968.
549 Suzuki, H., Shiokawa, K., Tsutsumi, M., Nakamura, T., & Taguchi, M. (2008). Atmospheric
550 gravity waves identified by ground-based observations of the intensity and rotational
551 temperature of OH airglow. *Polar science*, *2*(1), 1-8.
552 Tardelli-Coelho, F., Pimenta, A., Tardelli, A., Abalde, J., & Venkatesh, K. (2017). Plasma blobs
553 associated with plasma bubbles observed in the Brazilian sector. *Advances in Space*
554 *Research*, *60*(8), 1716–1724.
555 Takahashi, N., Seki, K., Teramoto, M., Fok, M. C., Zheng, Y., Matsuoka, A., ... & Nagatsuma,
556 T. (2018). Global distribution of ULF waves during magnetic storms: Comparison of
557 Arase, ground observations, and BATSRUS+ CRCM simulation. *Geophysical Research*
558 *Letters*, *45*(18), 9390-9397.
559 Takahashi, H., Figueiredo, C. A., Essien, P., Wrasse, C. M., Barros, D., Nyassor, P. K., ... &
560 Sampaio, A. H. (2022, December). Signature of gravity wave propagations from the
561 troposphere to ionosphere. In *Annales Geophysicae* (Vol. 40, No. 6, pp. 665-672).
562 Copernicus GmbH.
563 Wang, Z., Liu, H., Shi, J., Wang, G., & Wang, X. (2019). Plasma blobs concurrently observed
564 with bubbles in the Asian-Oceanian sector during solar maximum. *Journal of*
565 *Geophysical Research: Space Physics*, *124*(8), 7062–7071.

Wang, Z., Shi, J., Torkar, K., Wang, G., & Wang, X. (2015). A case study on ionospheric scintillations at low latitude associated with a plasma blob observed in situ. *Geophysical Research Letters*, *42*(7), 2109–2114.

Watanabe, S., & Oya, H. (1986). Occurrence characteristics of low latitude ionosphere irregularities observed by impedance probe on board the Hinotori satellite. *Journal of Geomagnetism and Geoelectricity*, *38*(2), 125–149.

Wickham, H. (2020). *Contours of a 2D density estimate - geom_density_2d*. - geom_density_2d • ggplot2. https://ggplot2.tidyverse.org/reference/geom_density_2d.html

Yokoyama, T., Su, S., & Fukao, S. (2007). Plasma blobs and irregularities concurrently observed by ROCSAT-1 and Equatorial Atmosphere Radar. *Journal of Geophysical Research: Space Physics*, *112*(A5).

Figure 1.

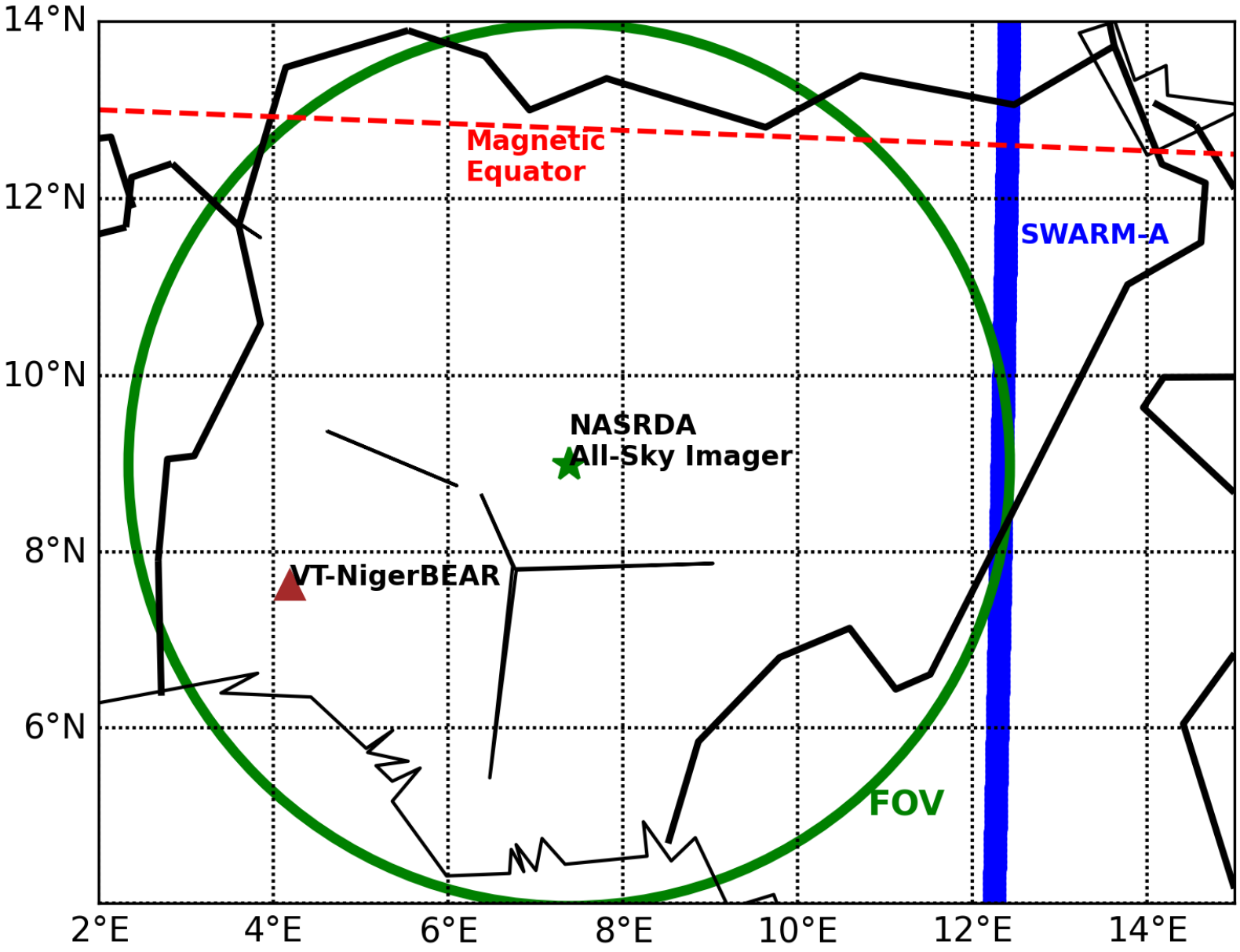
14°N
12°N
10°N
8°N
6°N
2°E
4°E
6°E
8°E
10°E
12°E
14°E
Magnetic
Equator
SWARM-A
NASRDA
All-Sky Imager
VT-NigerBEAR
FOV

Figure 2.

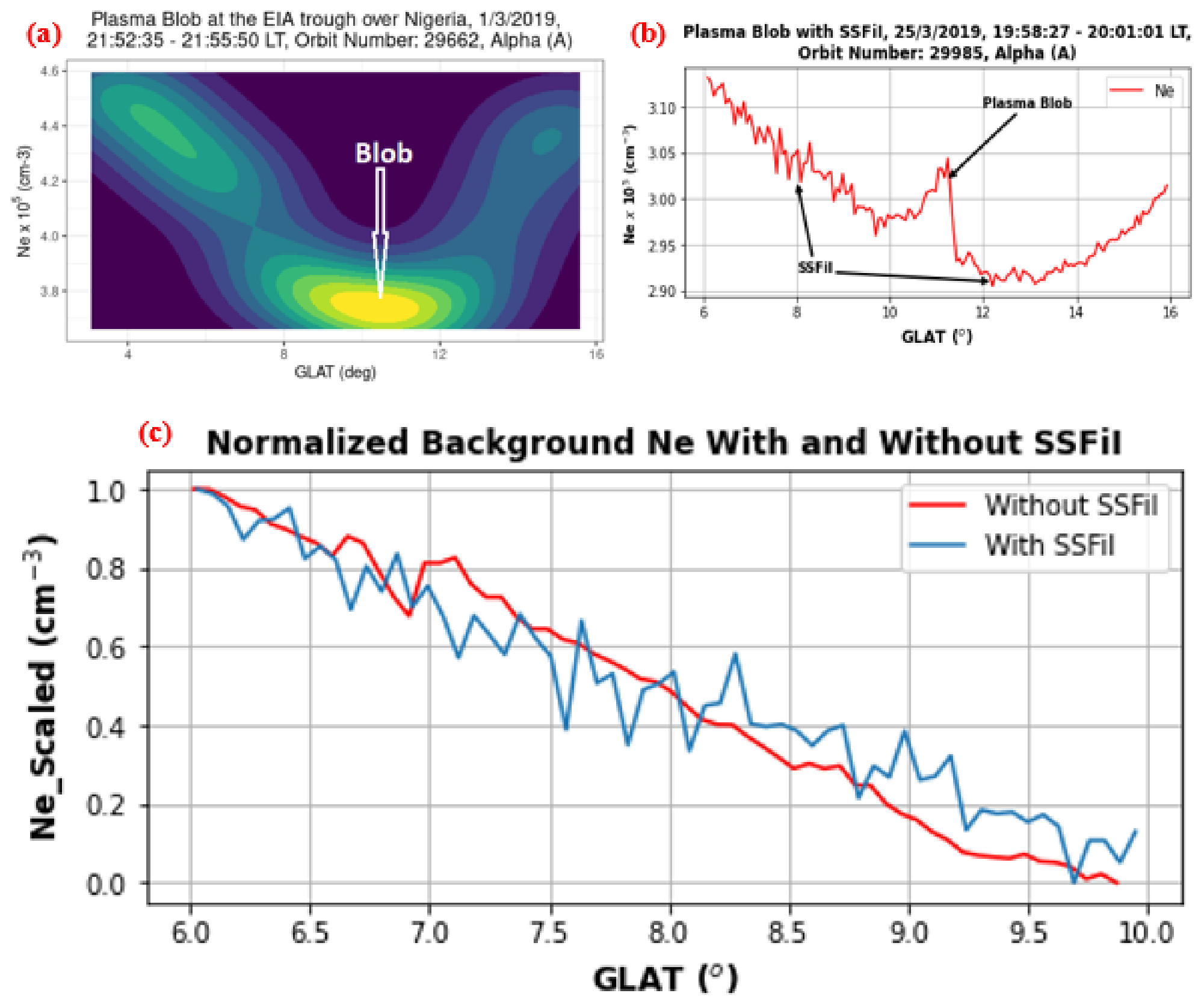
(a)
Plasma Blob at the EIA trough over Nigeria, 1/3/2019,
21:52:35 - 21:55:50 LT, Orbit Number: 29662, Alpha (A)
Blob
Ne x 10^5 (cm-3)
GLAT (deg)
(b)
Plasma Blob with SSFil, 25/3/2019, 19:58:27 - 20:01:01 LT,
Orbit Number: 29985, Alpha (A)
Ne
Plasma Blob
SSFil
Ne x 10^3 (cm^-3)
GLAT (°)
(c)
Normalized Background Ne With and Without SSFil
Without SSFil
With SSFil
Ne_Scaled (cm^-3)
GLAT (°)

Figure 3.

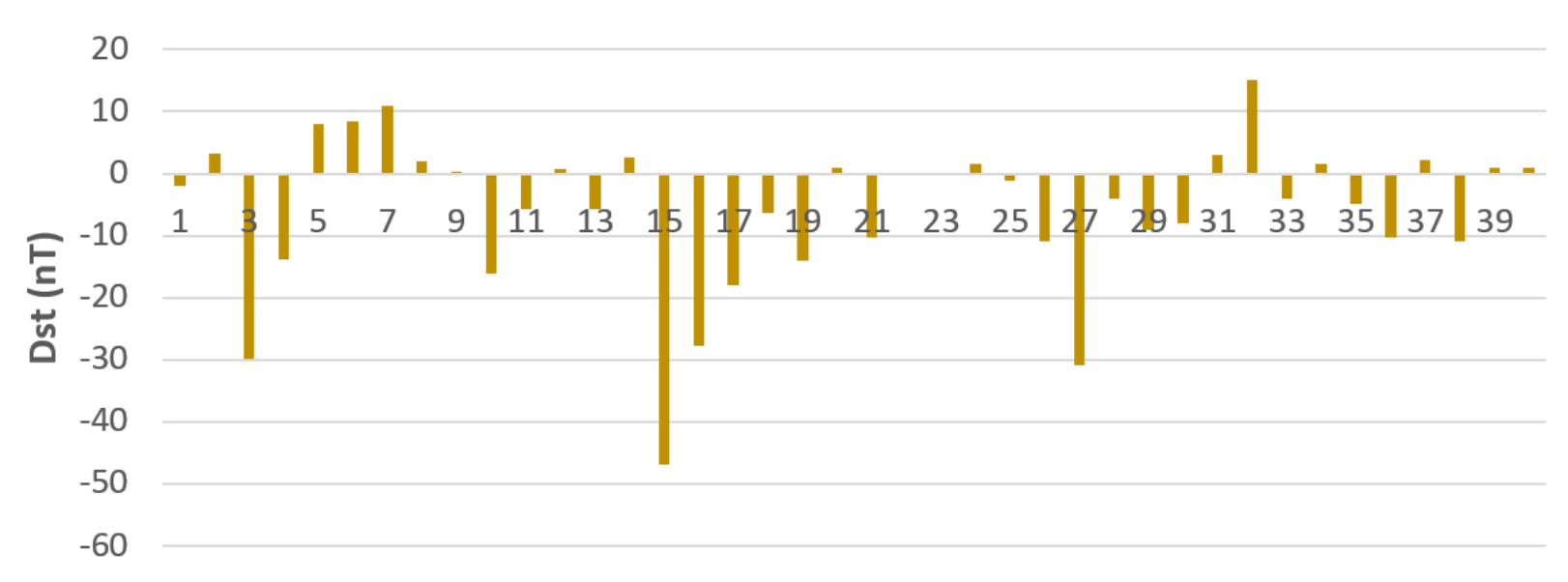
20
10
0
-10
-20
-30
-40
-50
-60
Dst (nT)
1
3
5
7
9
11
13
15
17
19
21
23
25
27
29
31
33
35
37
39

Figure 4.

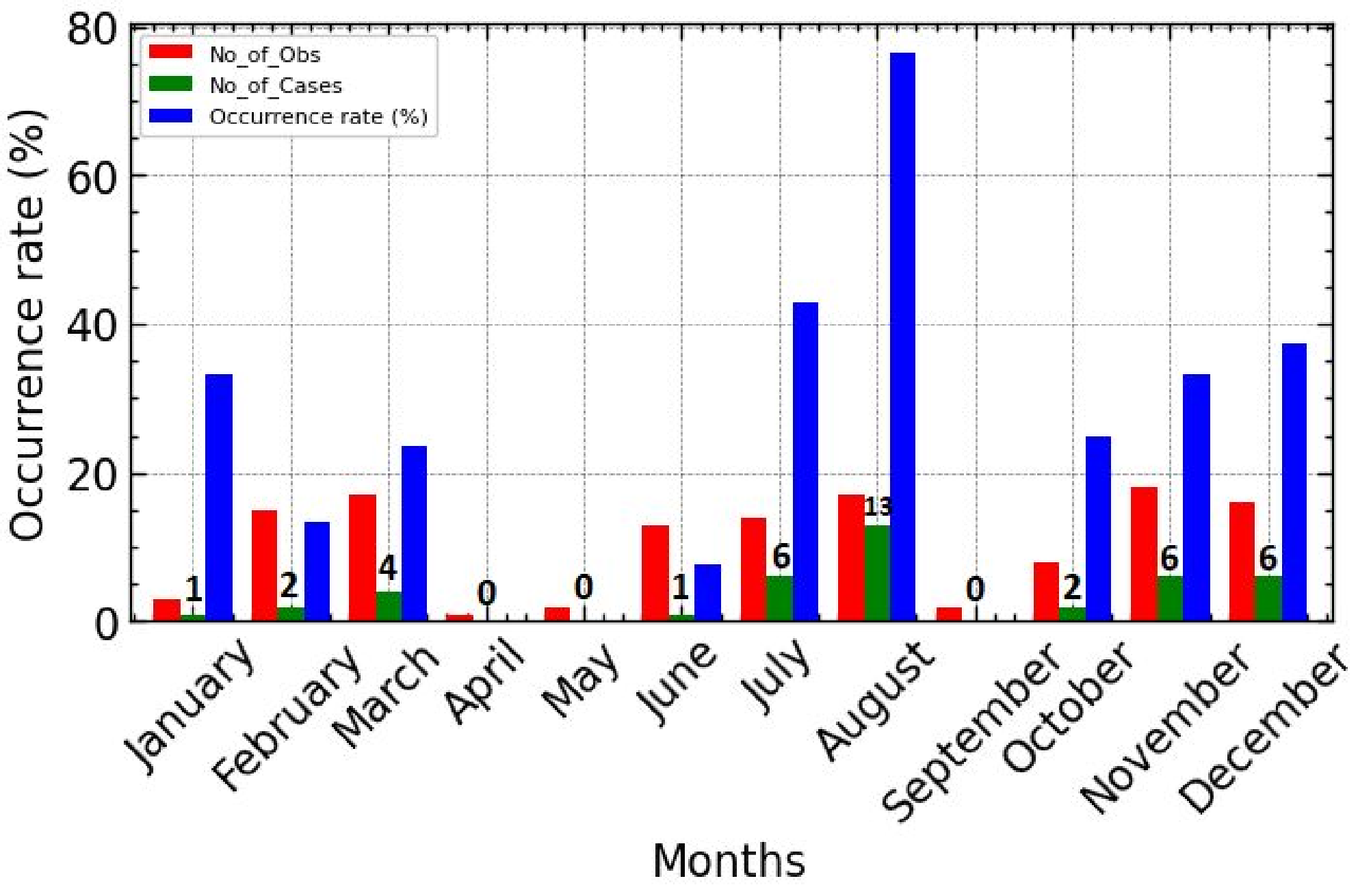
No_of_Obs
No_of_Cases
Occurrence rate (%)
Occurrence rate (%)
0
20
40
60
80
1
2
4
0
0
1
6
13
0
2
6
6
January
February
March
April
May
June
July
August
September
October
November
December
Months

Figure 5.

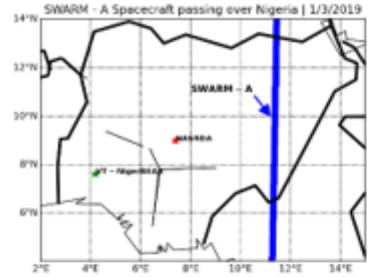
SWARM - A Spacecraft passing over Nigeria | 1/3/2019
SWARM – A
BASRDA
NigeriaSAT-X

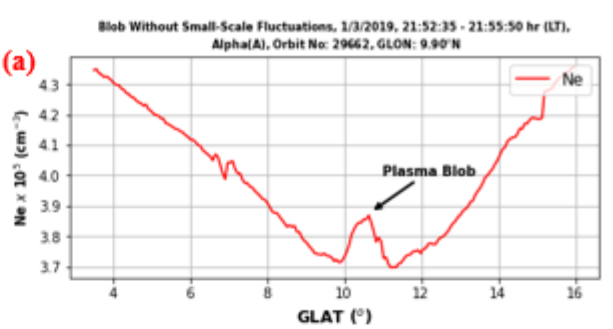
Blob Without Small-Scale Fluctuations, 1/3/2019, 21:52:35 - 21:55:50 hr (LT),
Alpha(A), Orbit No: 29662, GLON: 9.90°N
(a)
Ne
Plasma Blob
Ne x 10⁵ (cm⁻³)
GLAT (°)

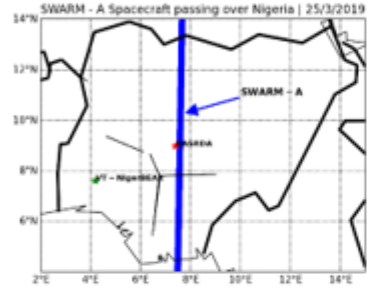
SWARM - A Spacecraft passing over Nigeria | 25/3/2019
SWARM – A
BASRDA
NigeriaSAT-X

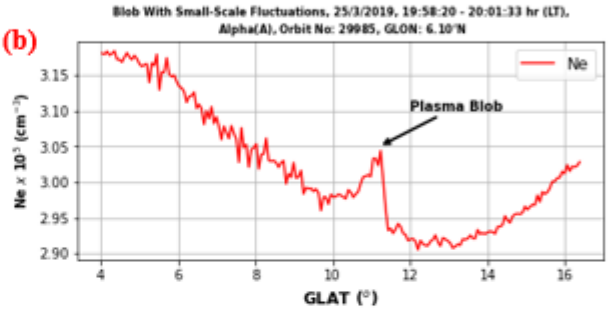
Blob With Small-Scale Fluctuations, 25/3/2019, 19:58:20 - 20:01:33 hr (LT),
Alpha(A), Orbit No: 29985, GLON: 6.10°N
(b)
Ne
Plasma Blob
Ne x 10⁵ (cm⁻³)
GLAT (°)

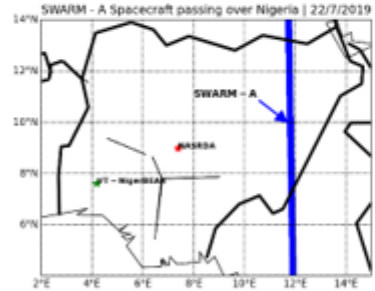
SWARM - A Spacecraft passing over Nigeria | 22/7/2019
SWARM – A
BASRDA
NigeriaSAT-X

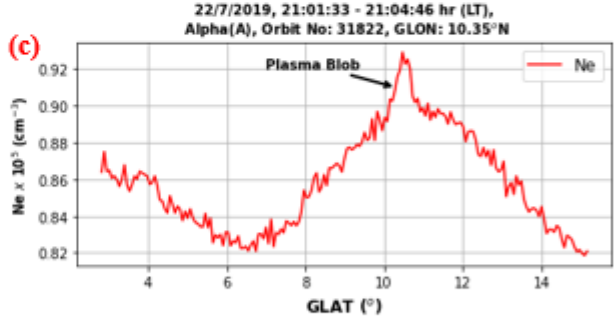
22/7/2019, 21:01:33 - 21:04:46 hr (LT),
Alpha(A), Orbit No: 31822, GLON: 10.35°N
(c)
Ne
Plasma Blob
Ne x 10⁵ (cm⁻³)
GLAT (°)

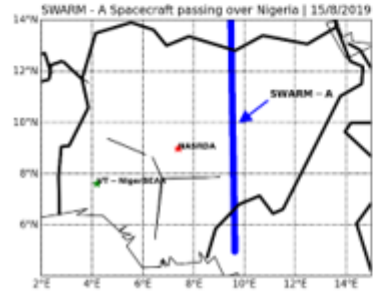
SWARM - A Spacecraft passing over Nigeria | 15/8/2019
SWARM – A
BASRDA
NigeriaSAT-X

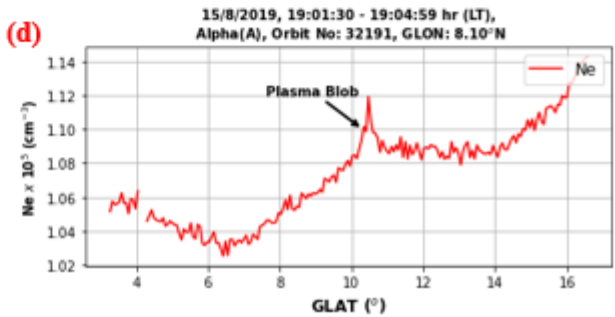
15/8/2019, 19:01:30 - 19:04:59 hr (LT),
Alpha(A), Orbit No: 32191, GLON: 8.10°N
(d)
Ne
Plasma Blob
Ne x 10⁵ (cm⁻³)
GLAT (°)

Figure 6.

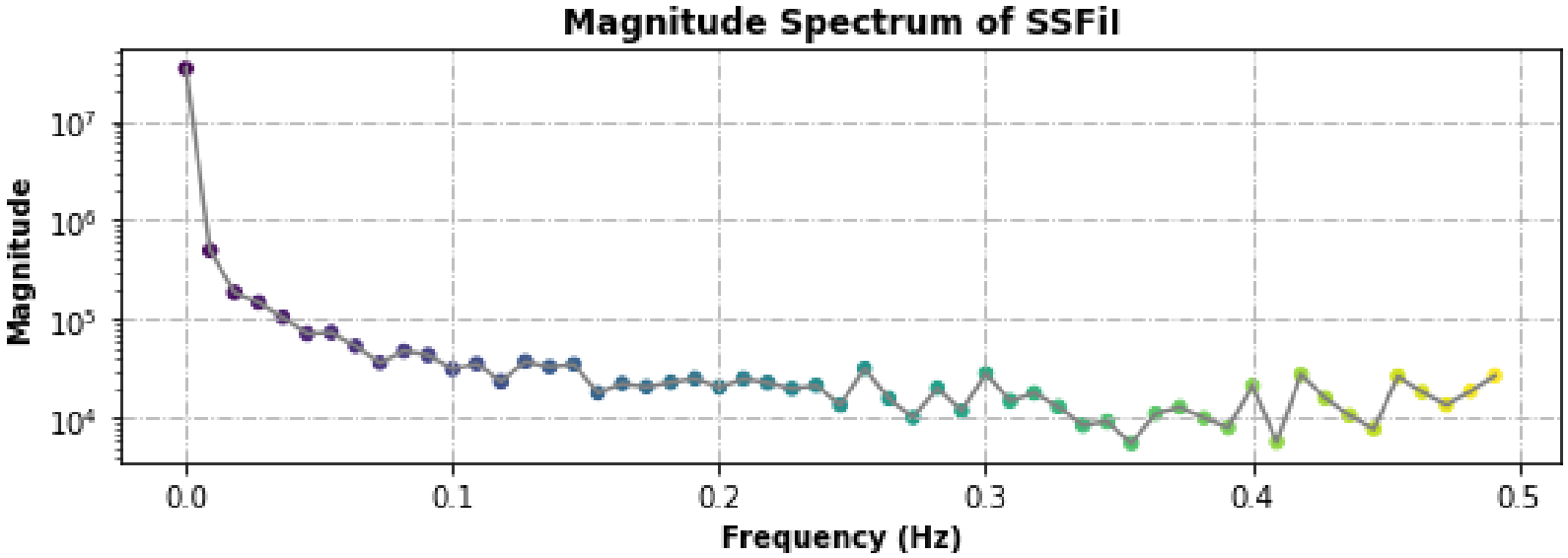
Magnitude Spectrum of SSFil
Magnitude
10^7
10^6
10^5
10^4
0.0
0.1
0.2
0.3
0.4
0.5
Frequency (Hz)

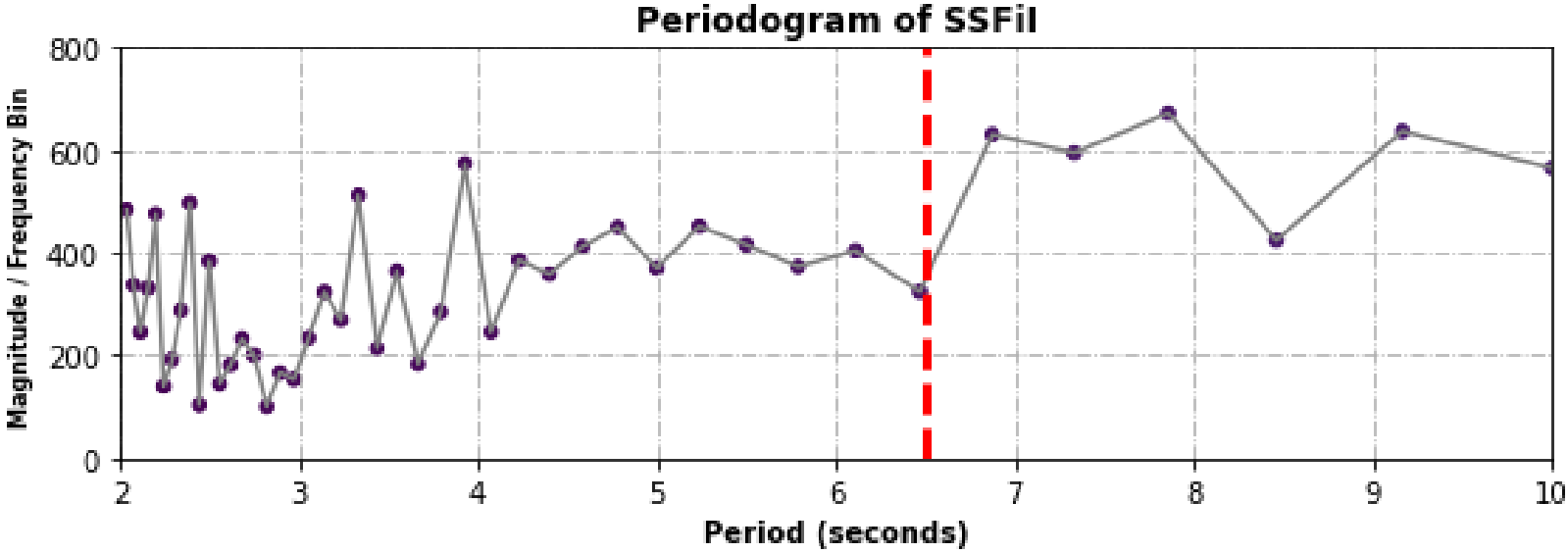
Periodogram of SSFil
Magnitude / Frequency Bin
800
600
400
200
0
2
3
4
5
6
7
8
9
10
Period (seconds)

Figure 7.

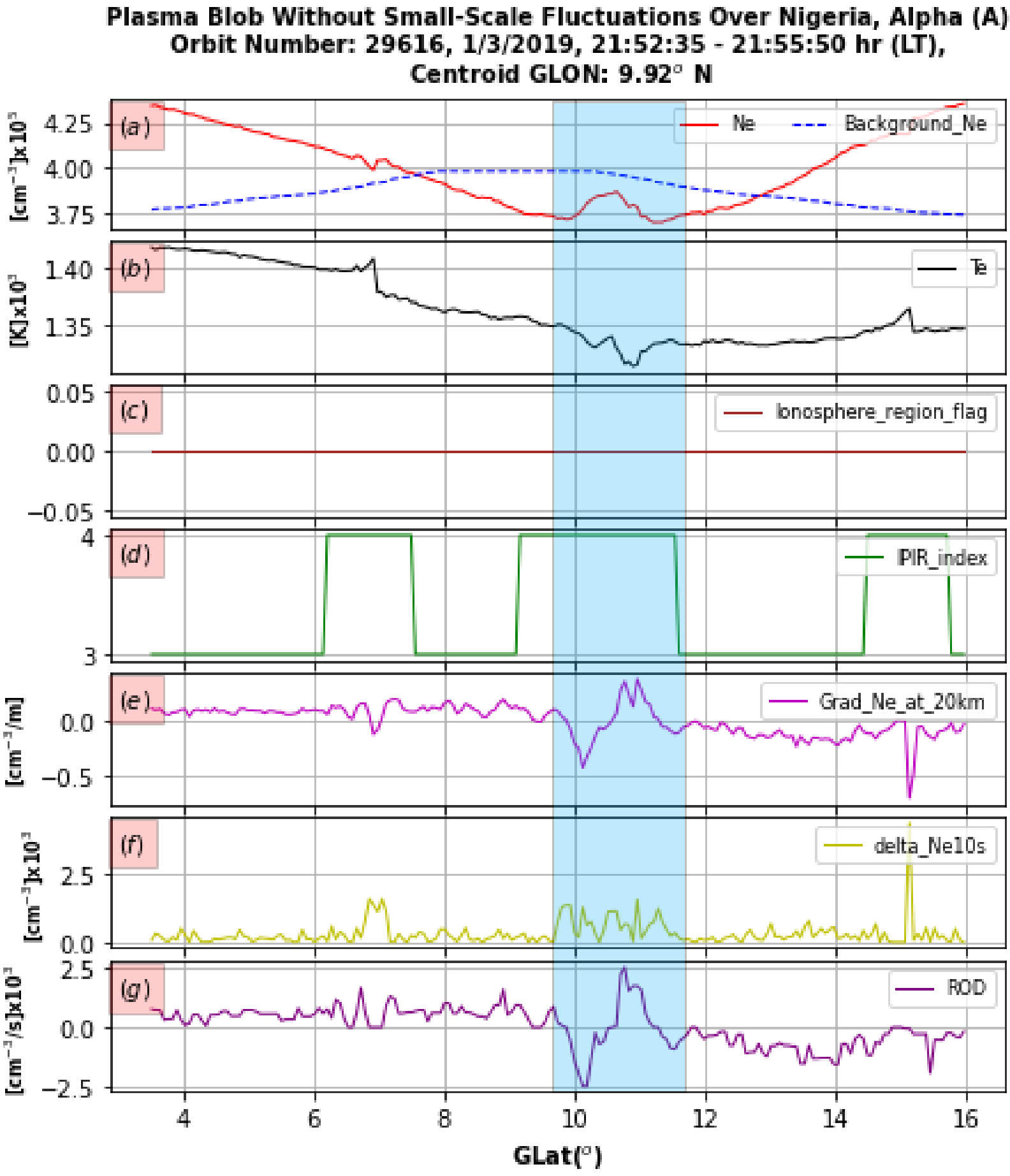
Plasma Blob Without Small-Scale Fluctuations Over Nigeria, Alpha (A)
Orbit Number: 29616, 1/3/2019, 21:52:35 - 21:55:50 hr (LT),
Centroid GLON: 9.92° N
(a)
Ne
Background_Ne
[cm⁻³]x10³
4.25
4.00
3.75
(b)
Te
[K]x10²
1.40
1.35
(c)
Ionosphere_region_flag
0.05
0.00
−0.05
(d)
IPIR_index
4
3
(e)
Grad_Ne_at_20km
[cm⁻³/m]
0.0
−0.5
(f)
delta_Ne10s
[cm⁻³]x10³
2.5
0.0
(g)
ROD
[cm⁻³/s]x10²
2.5
0.0
−2.5
4
6
8
10
12
14
16
GLat(°)

Figure 8.

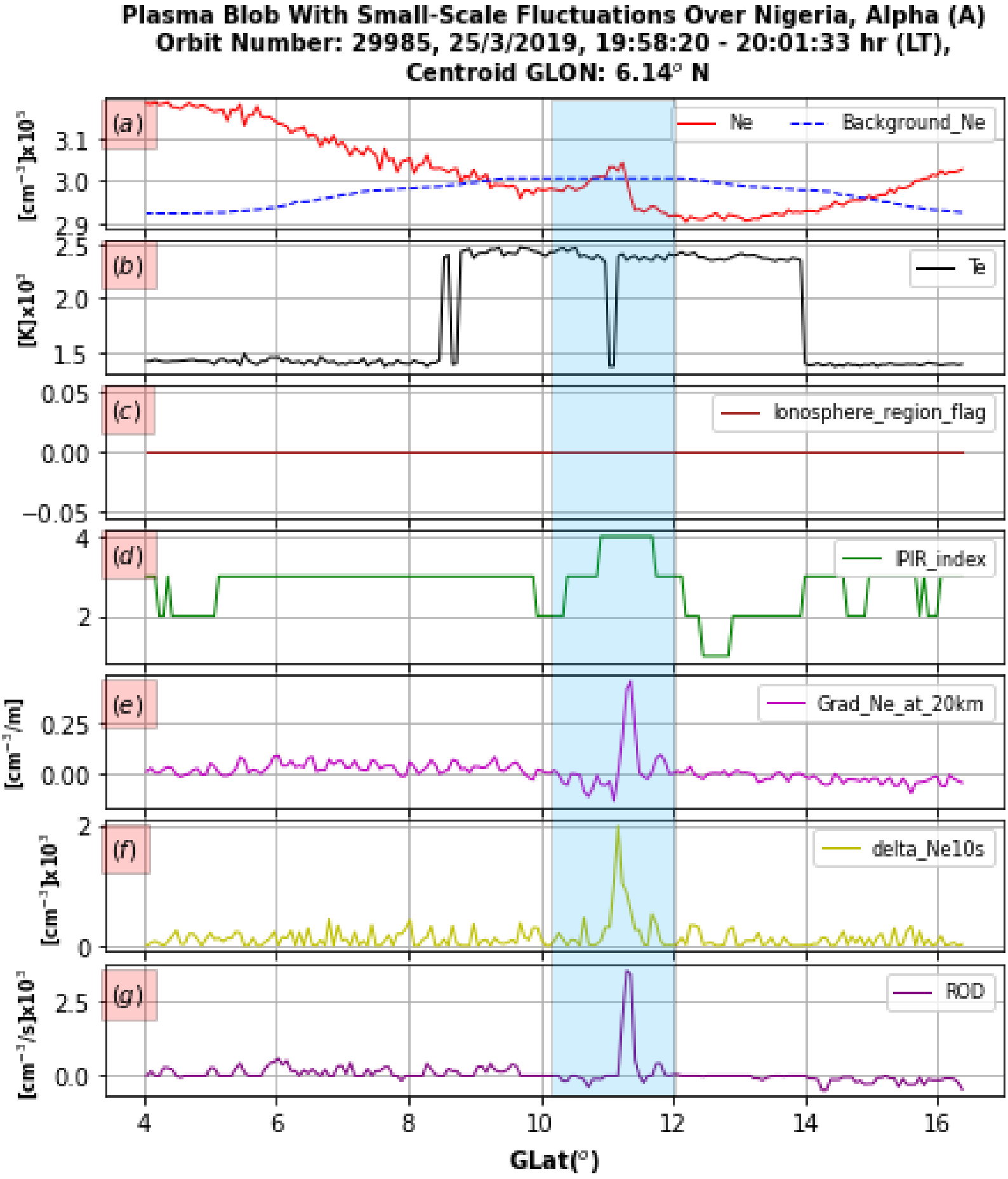
Plasma Blob With Small-Scale Fluctuations Over Nigeria, Alpha (A)
Orbit Number: 29985, 25/3/2019, 19:58:20 - 20:01:33 hr (LT),
Centroid GLON: 6.14° N
(a)
Ne
Background_Ne
[cm⁻³]x10³
3.1
3.0
2.9
(b)
Te
[K]x10³
2.5
2.0
1.5
(c)
Ionosphere_region_flag
0.05
0.00
−0.05
(d)
IPIR_index
4
2
(e)
Grad_Ne_at_20km
[cm⁻³/m]
0.25
0.00
(f)
delta_Ne10s
[cm⁻³]x10³
2
0
(g)
ROD
[cm⁻³/s]x10³
2.5
0.0
4
6
8
10
12
14
16
GLat(°)

Figure 9.

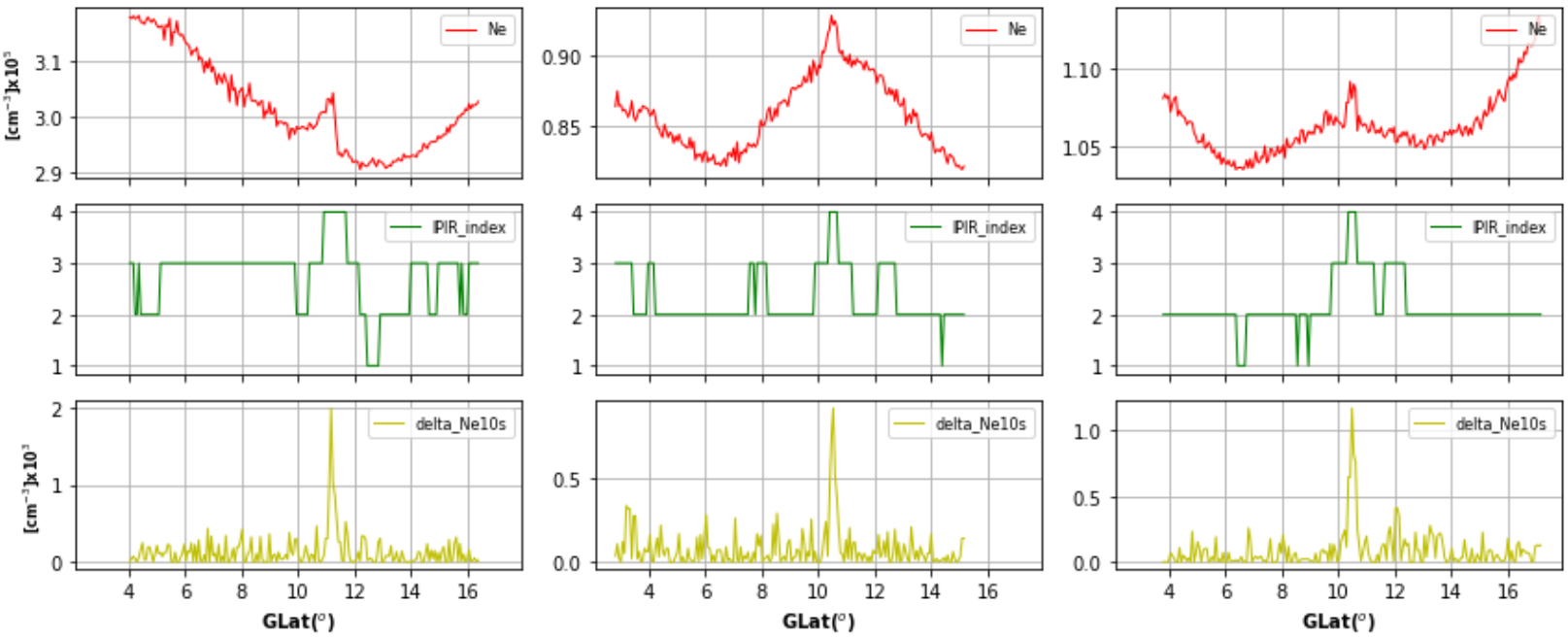
Ne
IPIR_index
delta_Ne10s
[cm⁻³]x10³
GLat(°)

Figure 10.

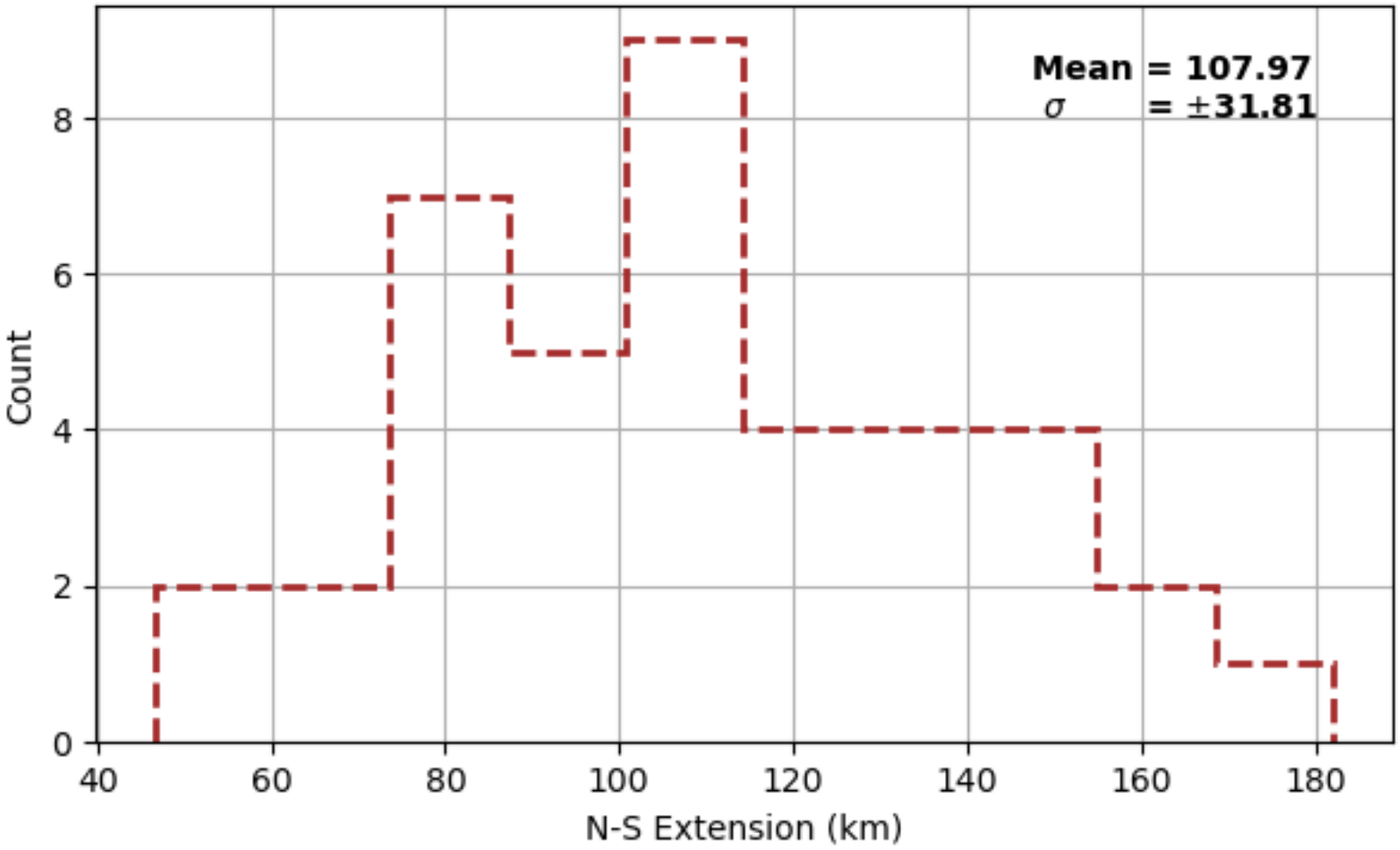
Mean = 107.97
σ = ±31.81
Count
N-S Extension (km)
0
2
4
6
8
40
60
80
100
120
140
160
180

Table 1: IPIR Dataset parameters used for this study. Twelve parameters are considered for this study, and their details are shown in the table.

S/N	Name	Description	Unit
1	Timestamp	CDF epoch of the measurement	-
2	Latitude	Position in ITRF – Latitude	degree
3	Longitude	Position in ITRF – Longitude	degree
4	Ne	Electron density, ne; downsampled to 1 Hz	cm^{-3}
5	Background_Ne	Background electron density, ne,b	cm^{-3}
6	Te	Electron temperature, Te; downsampled to 1 Hz	K
7	Grad_Ne_at_20 km	The electron density gradient over 20 km based on 2 Hz data	cm^{-3}/m
8	ROD	Rate Of change of density, dn/dt	cm^{-3}/s
9	delta_Ne10s	Fluctuation amplitudes over the baseline of 10 seconds	cm^{-3}
10	IBI_flag	Plasma Bubble Index, copied from the Level-2 Ionospheric Bubble Index product, IBIxTMS_2F	-
11	Ionosphere_region_flag	Determining the geomagnetic region where the measurement was taken (0: equator, 1: mid-latitudes; 2: auroral oval; 3: polar cap)	-
12	IPIR_index	Determining the level of fluctuations in the ionospheric plasma density	-

Table 2: Blobs statistical parameters monthly. The average of each of the cases is summarized in the table.

Months	**No_of _Obs**	**No_of_ Cases**	**Occurrence (%)**	**Density (10^5 cm^{-3})**	**N-S Extension (km)**	**GLAT (^{o})**	**GLON (^{o})**
January	3	1	33.3	0.987	132.10	10.45	15.35
February	15	2	13.3	2.501	77.70	10.38	15.13
March	17	4	23.5	3.432	129.32	10.82	10.19
April	1	0	0.0	-	-	-	-
May	2	0	0.0	-	-	-	-
June	13	1	7.7	2.094	57.72	10.87	5.54
July	14	6	42.9	1.796	93.06	10.76	8.06
August	17	13	76.5	2.331	107.58	10.74	8.90
September	2	0	0.0	-	-	-	-
October	8	2	25.0	2.229	112.11	10.57	9.42
November	18	6	33.3	2.374	120.62	10.28	12.61
December	16	6	37.5	2.103	94.54	10.47	13.66